A computational model tracks whole-lung *Mycobacterium tuberculosis* infection and predicts factors that inhibit dissemination

Authors:

Timothy Wessler[1,2#], Louis R. Joslyn[1,2#], H. Jacob Borish[3], Hannah P. Gideon[3], JoAnne L. Flynn[3], Denise E. Kirschner[2*], Jennifer J. Linderman[1*]

*Kirschner (kirschne@umich.edu) and Linderman (linderma@umich.edu) are co-corresponding.

#Wessler and Joslyn are co-first authors

Affiliations:

[1] Department of Chemical Engineering, University of Michigan, Ann Arbor, MI, United States

[2] Department of Microbiology and Immunology, University of Michigan, Ann Arbor, MI, United States

[3] Department of Microbiology and Molecular Genetics, University of Pittsburgh School of Medicine, Pittsburgh, PA, United States

Abstract

Mycobacterium tuberculosis (Mtb), the causative infectious agent of tuberculosis (TB), kills more individuals per year than any other infectious agent. Granulomas, the hallmark of Mtb infection, are complex structures that form in lungs, composed of immune cells surrounding bacteria, infected cells, and a caseous necrotic core. While granulomas serve to physically contain and immunologically restrain bacteria growth, some granulomas are unable to control Mtb growth, leading to bacteria and infected cells leaving the granuloma and disseminating, either resulting in additional granuloma formation (local or non-local) or spread to airways or lymph nodes. Dissemination is associated with development of active TB. It is challenging to experimentally address specific mechanisms driving dissemination from TB lung granulomas. Herein, we develop a novel hybrid multi-scale computational model, *MultiGran,* that tracks Mtb infection within multiple granulomas in an entire lung. *MultiGran* follows cells, cytokines, and bacterial populations within each lung granuloma throughout the course of infection and is calibrated to multiple non-human primate (NHP) cellular, granuloma, and whole-lung datasets. We show that *MultiGran* can recapitulate patterns of *in vivo* local and non-local dissemination, predict likelihood of dissemination, and predict a crucial role for multifunctional CD8+ T cells and macrophage dynamics for preventing dissemination.

Author Summary

Tuberculosis (TB) is caused by infection with *Mycobacterium tuberculosis* (Mtb) and kills 3 people per minute worldwide. Granulomas, spherical structures composed of immune cells surrounding bacteria, are the hallmark of Mtb infection and sometimes fail to contain the bacteria and disseminate, leading to further granuloma growth within the lung environment. To date, the

47 mechanisms that determine granuloma dissemination events have not been characterized. We
48 present a computational multi-scale model of granuloma formation and dissemination within
49 primate lungs. Our computational model is calibrated to multiple experimental datasets across
50 the cellular, granuloma, and whole-lung scales of non-human primates. We match to both
51 individual granuloma and granuloma-population datasets, predict likelihood of dissemination
52 events, and predict a critical role for multifunctional CD8+ T cells and macrophage-bacteria
53 interactions to prevent infection dissemination.
54

55 ## Introduction

56

57 Tuberculosis (TB) kills more individuals per year than any other infectious disease and treatment
58 remains a global challenge (1). Only a small fraction (5-10%) of those infected with
59 *Mycobacterium tuberculosis* (Mtb) develop active symptomatic disease (2), while the remainder
60 control but do not eliminate the infection, which is termed latent TB (LTBI). A hallmark of Mtb
61 infection is the presence of lung granulomas (lesions), collections of immune cells that surround
62 Mtb in an effort to contain and control an infection. Multiple granulomas can be present in
63 humans and non-human primates (NHPs). In NHPs, each granuloma is initiated by a single
64 bacillus (3). Of key importance is that each granuloma within an individual has its own
65 independent trajectory behavior. For example, the immune response in some granulomas
66 eliminates all bacteria, resulting in sterilization. In other granulomas, immune cells only contain
67 Mtb growth, resulting in stable granulomas that may persist for decades (4). If Mtb growth is not
68 contained, however, granulomas can grow and/or spread, allowing for dissemination of bacteria
69 across the lungs leading to the formation of new granulomas, spread to the airways resulting in

70 transmission of infection through aerosolized bacteria, and possibly death of the host if not
71 treated. Understanding the collective behavior of granulomas within lungs leading to
72 dissemination events is critical to the ultimate goal of controlling the global TB epidemic.
73
74 It is difficult to experimentally address specific mechanisms operating within lungs that drive
75 different granuloma outcomes in primates, although it is known through interventional studies
76 that certain factors, such as TNF, CD4+ T cells, and CD8+ T cells are important in controlling
77 early and established Mtb infection (5–8). As a complementary approach, mathematical
78 modeling can generate hypotheses that can then be tested experimentally. Several mathematical
79 and computational models for Mtb infection have been developed to explore the contributions of
80 the innate and adaptive immune responses to granuloma formation and function (9–20). These
81 models are informed by studies in humans and in animal models of infection, especially NHPs,
82 rabbits, pigs, and mice (21). In particular, *GranSim,* our computational model that allows
83 simulation of the formation and function of a single granuloma using a hybrid agent-based model
84 framework, has offered strategies for drug treatment and vaccine development (12,14,22–24).
85 *GranSim*, which considers thousands of cells and bacteria as "agents" in the simulation and
86 tracks diffusion of multiple immune mediators (e.g., cytokines), is computationally intensive,
87 limiting our ability to simultaneously simulate multiple granulomas present in an entire lung
88 during infection. In contrast, Prats et al. (18) utilized a bubble model to demonstrate the
89 importance of local inflammation, dissemination, and coalescence of lesions as key factors
90 leading to active TB, but did not specifically model events at the granuloma scale. However,
91 following the formation of individual granulomas, the dissemination of those granulomas across
92 the lungs over time, and, importantly, tracking events at the granuloma scale could provide an

93 important window into infection dynamics and could lead to new insights for prevention or
94 treatment.
95
96 In order to study the formation of new granulomas after initial establishment of infection,
97 referred to as dissemination, the evolution of individual granulomas must be captured over time.
98 Recently, research on Mtb-infected NHPs provided data on disseminating granulomas (25). Of
99 all animal models used to study Mtb infection, NHPs are most relevant to human TB disease
100 because they recapitulate the full spectrum of clinical outcomes and pathologies seen in humans
101 (26). From PET CT imaging, the emergence of new granulomas was tracked and recorded. The
102 authors genetically matched Mtb barcodes, assigned each inoculation Mtb a unique barcode ID,
103 and associated each granuloma identified in the temporal PET CT images with the Mtb barcodes
104 inside that granuloma (Figure 1). By identifying Mtb barcodes that were present in multiple
105 granulomas, they were able to distinguish disseminating from non-disseminating granulomas.
106 When identifying multiple bacterial barcodes within a single granuloma, it is surmised a merger
107 of granulomas took place. While Martin et al. showed these distinctions, the mechanisms that
108 lead to granuloma clustering or dissemination remain unanswered. We address these open
109 questions using a hybrid computational-mathematical modeling framework.
110
111
112 **Fig 1. Three NHP lung maps illustrating the positioning of pulmonary granulomas and**
113 **thoracic lymph nodes (data previously published in Martin et al. (22)).** Gray outlines denote
114 the extent of the lungs, bronchial tubes, and trachea. Small markers superimposed on the outlines
115 represent the positions of pulmonary granulomas, while larger markers denote lymph nodes.
116 Colors denote unique barcode tags. Some samples had more than one barcode tag present, and
117 often these were doublet granulomas (i.e., two granulomas too close in proximity to distinguish
118 at necropsy) and so are marked with a pie chart showing the relative abundance of each barcode
119 tag. The black markers represent pulmonary granulomas for which no barcode tags were found.

Filled black markers are granulomas which grew bacteria upon plating but barcodes could not be determined for technical reasons, while open markers are granulomas that did not grow bacteria upon plating (sterile).

Herein, we develop a novel multi-scale hybrid model, *MultiGran,* to track Mtb infection at the scale of the entire lung, including capturing multiple granulomas and their individual outcomes as well as the formation of new granulomas. *MultiGran* is an agent-based model that follows cells, cytokines, and bacterial populations across multiple lung granulomas throughout the course of infection. Each granuloma is now formulated as a single agent, and each agent contains within it a system of non-linear ordinary differential equations (ODEs) that capture individual granuloma dynamics. *MultiGran* follows the steps observed through the course of Mtb infection: (1) *initial granuloma establishment* with Mtb that have been virtually barcoded and placed within the lung environment, (2) *granuloma development* across time, (3) the possibility of *granuloma dissemination* with barcoded bacteria moving to a new location, and (4) *granuloma merging* by granulomas that have formed close together and whose individual boundaries are indistinguishable, or those that grow in size and thus merge into a granuloma cluster (that may have multiple barcoded bacteria IDs). We use *MultiGran* to address three outstanding questions about dissemination: what mechanisms are consistent with granuloma dissemination and merging patterns seen *in vivo*? What is the likelihood of a granuloma to disseminate? Can we predict factors that lead to dissemination?

Methods

Ethics Statement

All experimental manipulations, protocols, and care of the animals were approved by the

University of Pittsburgh School of Medicine Institutional Animal Care and Use Committee (IACUC). The protocol assurance number for our IACUC is A3187-01. Our specific protocol approval numbers for this project are 1280653, 12126588, 11110045, 19024273, 15066174, 16017309 and 18124275. The IACUC adheres to national guidelines established in the Animal Welfare Act (7 U.S.C. Sections 2131 - 2159) and the Guide for the Care and Use of Laboratory Animals (8th Edition) as mandated by the U.S. Public Health Service Policy.

All macaques used in this study were housed at the University of Pittsburgh in rooms with autonomously controlled temperature, humidity, and lighting. Animals were singly housed in caging at least 2 square meters apart that allowed visual and tactile contact with neighboring conspecifics. The macaques were fed twice daily with biscuits formulated for NHPs, supplemented at least 4 days/week with large pieces of fresh fruits or vegetables. Animals had access to water *ad libitem*. Because our macaques were singly housed due to the infectious nature of these studies, an enhanced enrichment plan was designed and overseen by our nonhuman primate enrichment specialist. This plan has three components. First, species-specific behaviors are encouraged. All animals have access to toys and other manipulata, some of which will be filled with food treats (e.g., frozen fruit, peanut butter). These are rotated on a regular basis. Puzzle feeders foraging boards, and cardboard tubes containing small food items also are placed in the cage to stimulate foraging behaviors. Adjustable mirrors accessible to the animals stimulate interaction between animals. Second, routine interaction between humans and macaques are encouraged. These interactions occur daily and consist mainly of small food objects offered as enrichment and adhere to established safety protocols. Animal caretakers are encouraged to interact with the animals (by talking or with facial expressions) while performing

168 tasks in the housing area. Routine procedures (e.g., feeding, cage cleaning) are done on a strict
169 schedule to allow the animals to acclimate to a routine daily schedule. Third, all macaques are
170 provided with a variety of visual and auditory stimulation. Housing areas contain either radios or
171 TV/video equipment that play cartoons or other formats designed for children for at least 3 hours
172 each day. The videos and radios are rotated between animal rooms so that the same enrichment is
173 not played repetitively for the same group of animals.
174
175 All animals are checked at least twice daily to assess appetite, attitude, activity level, hydration
176 status, etc. Following Mtb infection, the animals are monitored closely for evidence of disease
177 (e.g., anorexia, weight loss, tachypnea, dyspnea, coughing). Physical exams, including weights,
178 are performed on a regular basis. Animals are sedated prior to all veterinary procedures (e.g.,
179 blood draws) using ketamine or other approved drugs. Regular PET/CT imaging is conducted on
180 most of our macaques following infection and has proved very useful for monitoring disease
181 progression. Our veterinary technicians monitor animals especially closely for any signs of pain
182 or distress. If any are noted, appropriate supportive care (e.g., dietary supplementation,
183 rehydration) and clinical treatments (analgesics) are given. Any animal considered to have
184 advanced disease or intractable pain or distress from any cause is sedated with ketamine and then
185 humanely euthanatized using sodium pentobarbital.
186
187 ***Experimental dataset***
188 Experimental data specifically for this study were obtained from seven cynomolgus macaques
189 (*Macaca fascicularis*), infected with low dose Mtb (Erdman strain, ~10 CFU by bronchoscopic
190 instillation) as previously described (27–29). Infection was confirmed by PET CT imaging. PET

CT scans were performed monthly to quantify new granuloma formation or clustering, as well as disease progression. Necropsy was performed as previously described (28,29). Briefly, an ^{18}F-FDG PET-CT scan was performed on every animal 1-3 days prior to necropsy to measure disease progression and identify individual granulomas and other pathologies as described (27–30); this scan was used as a map for identifying individual lesions. At necropsy, each granuloma or other pathologies from lung and mediastinal lymph nodes were obtained for histological analysis, bacterial burden, and immunological studies, including flow cytometry, as previously described (27–30). For bacterial burden, each granuloma homogenate was plated onto 7H11 medium, and the CFU were enumerated 21 days later to determine the number of bacilli in each granuloma (27,29).

To calibrate the individual granuloma computational model, we excised granulomas from macaques that were infected for 3 weeks (n=2), 5 weeks (n=2), 7 weeks (n=2) and 9 weeks (n=1). In addition, an animal without Mtb infection was also included in this study as a control. To obtain accurate cell number measurements, enzymatic digestion (Tumor dissociation kit, human; Miltenyi Biotec) was performed on excised granulomas using gentleMACS octo dissociator. The single cell suspension obtained by enzymatic digestion was processed for bacterial burden and cell numbers enumeration (27). Single cell suspensions of individual granulomas were stained with cell surface antibodies to enumerate T cells (CD3) and macrophages (CD11b). The cells were further stained intracellularly with Calprotectin antibody to exclude CD11b+Calprotectin+ cells from macrophage population. Flow cytometry and data acquisition was performed using BD LSRII and analysis was performed using Flowjo Software v10 (27).

In addition, bacterial burden data of 623 granulomas from 38 NHP that were controls in other studies (previously published (20,27,31–33) and ongoing studies) at University of Pittsburgh (Flynn Lab) were included for evaluation. The timing of infection depended on the particular study (Table of CFU values and tables of cell counts located at http://malthus.micro.med.umich.edu/labmovies/MultiGran/) Table: gran-cfu-cyno-size) and ranged from 4-17 weeks post Mtb infection.

Non-human primate lung lattice data

To create a virtual lung that replicates an NHP lung, we used a CT scan of an uninfected NHP to model the 3-dimensional lung space. Binary images mapping the cross section of the lungs were created for each CT slice by segmentation of CT image values below -320 Houndsfield units. The individual slices were then stacked into an array, and a polygon mesh outlining the lung volume was generated using the marching_cubes_classic function in the open source Python scikit-image package (v 0.14.1, (34)).

Identifying granuloma distributions in Non-human primate lungs

To allow us to test whether the distribution of granulomas in our virtual lungs matched that observed in NHP lungs, we refer to the distribution of granulomas arising from barcoded bacteria derived from our previously published data in Martin et al. (25). In that study, four cynomolgus macaques were infected with 11+/- 5 CFU barcoded Mtb Erdman. Barcoded libraries were

generated where each bacterium has a different random 7-mer along with one of three 75-mer identifier tags inserted into the bacterial chromosome. This process created roughly 50,000 bacteria that are able to be uniquely identified by the random 7-mer tag with very small (< 2%) risk of duplication in an infection of <50 CFU (See Figure 1 in Martin et al. (25)). The animals were necropsied between 15 and 20 weeks post-infection. Animals were imaged at monthly intervals (or more frequently) to identify timing of granuloma establishment. Pulmonary granulomas were excised during necropsy, and their three-dimensional positions were recorded via matching to PET/CT imaging. Homogenates from excised pulmonary granulomas and infected thoracic lymph nodes were plated, scraped, and sequenced to identify the specific barcode(s) present in each granuloma. Matching the x, y, and z coordinates recorded for each granuloma with its determined barcode content led to a three-dimensional map of the locations of each barcode throughout the pulmonary space. Bacterial burden for each granuloma was determined by counting colonies on the plates.

Three of the four maps are shown in Figure 1 (the fourth was already presented in the original paper (25)). Lung outlines were calculated from terminal scans of each NHP by the process of creating a polygon mesh described above. Small markers represent pulmonary granulomas, while larger markers denote lymph nodes. Each color represents a unique barcode tag. Some samples had more than one barcode tag present, and often these were doublet granulomas (i.e., two granulomas too close in proximity to distinguish at necropsy) and so are marked with a pie chart showing the relative abundance of each barcode tag. The black markers represent pulmonary granulomas for which no barcode tags were found. Filled black markers are granulomas which grew bacteria upon plating but for which barcodes could not be determined, while open markers

258 are granulomas that did not grow bacteria upon plating (sterile); in this study, only CFU+
259 granulomas were available for barcode determination.
260
261 ***Model Overview***
262 *MultiGran* is a novel multi-scale, hybrid agent-based model that describes the formation,
263 function, and dissemination of lung granulomas containing Mtb (Figure 2). It uses sampling of
264 nonhomogeneous Poisson processes; rule-based agent placement; parameter randomization;
265 solving systems of non-linear ODEs; and post-process agent groupings to perform *in silico*
266 experiments that track the progress of infection in an individual host. Each granuloma (agent) is
267 placed stochastically within the boundary of the lung environment based on a set of rules. Within
268 each agent, a system of ODEs is linked internally and solved simultaneously to update
269 concentrations of cells, cytokines, and bacterial burdens within each granuloma at every time
270 step. Additionally, within every time step, each granuloma is given the opportunity to
271 disseminate locally and non-locally. *Local dissemination* involves a new granuloma being
272 initialized nearby, while *non-local dissemination* allows initialization anywhere within the lung
273 environment. At the lung scale, the model tracks the development, location, and quantity of
274 granulomas, and determines whether each granuloma is either alone or a member of a larger
275 granuloma cluster. At the granuloma scale, dissemination-event decisions, rules for granuloma
276 formation, and concentrations of all granuloma components are tracked and defined. As is
277 occasionally done when a flexible agent size is needed (35), our agents (granulomas) are placed
278 on a continuous grid. Agents are spherical with dynamically-changing sizes, and granuloma
279 clustering depends on the geometry and position of each of the agents.
280

Figure 2: Process of Mtb infection and rules for granuloma dissemination and placement within *MultiGran*.
(A) A nonhuman primate is inoculated with Mtb, here tracked using different "barcodes" or IDs. These Mtb are taken up by resident macrophages, initiating an innate immune response. This response includes the secretion of various cytokines and chemokines that help prime and/or recruit other immune cells to the site of the infection, resulting in the formation of lung granulomas. Occasionally, as a granuloma develops, it may disseminate--either locally or non-locally. In local dissemination, an Mtb-infected macrophage moves to another nearby location within the same lung lobe. In non-local dissemination, a free extracellular Mtb reaches the airways or is carried to a draining lymph node and then deposited at a site not necessarily near the original location; i.e., in a different lung lobe. Granuloma clusters can form when granulomas develop near each other and may grow into each other, or when one granuloma forms immediately adjacent to the original granuloma via local dissemination (3). Granuloma clusters may contain more than one Mtb ID. **(B)** The rules of granuloma establishment and dissemination within MultiGran. **Case 1 – inoculation.** Inoculation deposits bacteria in a specific lung region at position *(xTrial, yTrail, zTrial)*. The black box designates inoculation region (row 1), wherein the specific within-lung region destined for inoculation is highlighted in green (row 2). The third row demonstrates successful inoculation of a single bacterium – the black box was sampled randomly until the sampled coordinates lie within the green region. Cases 2 and 3 define granuloma placement following dissemination. **Case2 – non-local dissemination**. When non-local dissemination occurs, a bacterium escapes a single granuloma (row 1) and can be placed in any region (shown in black in row 2) that encompasses the entire lung. The green highlighted region is the area in which the bacterial placement will be accepted. Row 3 shows three trial placements: two realizations of accepted bacterial placement (black arrows) and one unaccepted placement (red arrow) at *(xTrial, yTrial, zTrial)*. **Case 3– local dissemination**. Local dissemination is the only form of granuloma placement which does not utilize random placement within a region of lung space. Rather, an infected macrophage from the parent granuloma is placed in a random direction away from the parent granuloma. Row 2 shows several options for granuloma infected macrophage placement. Note that the arrows are of different length to represent our assumption that local dissemination likely follows a normal distribution with respect to parent granuloma location. Here, the green and black arrows show valid directions for the new placement for the infected macrophage, while red arrows show invalid directions. A new granuloma will begin to develop in the chosen (green) valid location (Row 3). Note that in both **(A)** and **(B)** bacteria, granulomas, and infected macrophages are not to scale. Lung image from Servier Medical Art.

Each *in silico* experiment using *MultiGran* is designed to replicate an *in vivo* experiment. To replicate the studies by Martin et al. (25), our simulated NHP is infected with roughly 19

uniquely-identified (barcoded) Mtb that are randomly placed in a localized region of the lungs, similar to the typical inoculation process in the NHP experiments. Each Mtb is assumed to be immediately taken up by a resident lung macrophage, forming a single, unique new granuloma (25). Each granuloma evolves independently. Whenever a granuloma is formed, it is initialized with parameter values that represent several characteristics that ultimately influence its future behavior, as well as the emergent outcomes of the system as a whole.

Simulation Environment

Code is written in MATLAB, with Bash script for submission to run on computer clusters. ODEs are solved using MATLAB's ode15s with the NonNegative option for all terms, and we define the start and end time interval to be the size of the agent time step. To avoid complications with the random number generator seed being reset with the initialization of each MATLAB instance, the Bash script executes code that generates a randomized seed list for the simulation to use. The website http://malthus.micro.med.umich.edu/labmovies/MultiGran/ has pseudocode and implementation descriptions, as well as simulation videos.

Granuloma Establishment

A granuloma is initialized when Mtb is deposited into the lung environment. Based on our previous publications (3,25), we assume that each Mtb creates one granuloma (3,36). The granulomas established during inoculation (Figure 2B – Case 1) are referred to as "founder" granulomas and are considered first-generation granulomas; all other granulomas that may emerge throughout the simulation originate from these founders.

Granulomas are agents, so at initialization we assign parameter values to each granuloma and its infecting Mtb, as well as counts and concentrations of all cell types and cytokines. Every granuloma is assigned unique identification markers. These include being given a unique individual granuloma ID *IndivGranID(i)*, which is assigned in chronological order of initialization $i=1,2,...N$ (where N is the total number of granulomas), as well as the individual granuloma ID of its parent, so the lineage of each of the founder Mtb can be tracked throughout the course of infection. Each granuloma is also given a position on a continuous grid.

Granuloma Development

The development of each individual granuloma "agent" is captured by a set of ODEs with 16 equations for 16 state variables capturing bacterial, T cell, macrophage and cytokine dynamics (see Appendix 1 for equations and complete term-by-term description of the model). ODE model formulations build on our previous work (37–39) describing cells and levels of cytokines in a whole lung. The equations have been re-calibrated to NHP granuloma data (see section on Experimental dataset) to represent an individual granuloma (see section Model Parameters, Calibration, and Sensitivity Analysis), and have been updated in several ways. First, we increased the role of IL-10, including it as a factor for downregulating macrophage activation and TNF-α production by activated macrophages, as well as allowing infected macrophages to produce IL-10, based on NHP data (40–42). The other set of changes relates to intra- and extra-cellular Mtb to be consistent with recent findings on Mtb growth within macrophages (43–45). Rather than releasing the entire carrying capacity of bacteria at the occurrence of each death of an infected macrophage, the amount of intracellular Mtb within an average infected macrophage is released (with the exception of a bursting infected macrophage, in which case the maximum

amount of Mtb is released). Furthermore, only a fraction of intracellular Mtb released during the natural death of an infected macrophage survives to become an extracellular Mtb. The expression for intracellular Mtb replication was also changed along with the addition of an expression for the natural slow death of intracellular Mtb for model stability. We record granuloma sterilization when the count of Mtb drops below 0.5.

Granuloma Dissemination

While the mechanisms behind dissemination are not yet well-understood (25), we have created rules such that the emergent outcomes are consistent with experiments (Figure 2B). We define a probability function for likelihood of a dissemination event, which we make dependent on the bacterial load (CFU) of the granuloma. We selected CFU because the data presented by Lin et al. (3) indicates that granuloma carrying capacity has a limit (approximately 10^5). Because NHP granulomas rarely exceed this limit (3,28), there is likely a link between granuloma CFU and dissemination. Because Mtb is by itself non-motile, we consider two routes of dissemination: 1) Mtb conveyance within an infected macrophage and 2) a single Mtb flowing through lung airways or deposited via a draining lymph node (LN). From these, we incorporated two types of dissemination events: local and non-local, the probabilities of each event being independent, and in the unlikely event that multiple dissemination events occur in the same time step, the order of events is randomized.

When a granuloma disseminates locally (Figure 2B – Case 3), an infected macrophage carrying intracellular Mtb is assumed to move from the parent granuloma position to a new position nearby. We assume the distance between the parent granuloma and a new position likely follows

391 a normal distribution with respect to parent location and we calibrated the mean and variance of
392 this location using the data presented in Martin et al. (25). In Martin et al., the authors compute
393 distances of each granuloma and granuloma clusters that they could identify via PET/CT, rather
394 than every individual granuloma regardless of size and cluster affiliation. We also assume that a
395 pre-determined quantity of T cells moves with an infected macrophage. After this dissemination
396 event, the parent and daughter granulomas evolve independently from each other. When a
397 granuloma disseminates non-locally (Figure 2B – Case 2), an extracellular Mtb is simulated as if
398 entering airways (or via a LN) and deposited with equal likelihood anywhere within the lungs,
399 where it is immediately taken up by a macrophage. Figure 2B-Case 2 represents 3 realizations of
400 trial coordinates wherein the trial coordinates represented by the red arrow do not satisfy our
401 criteria, but the two black arrows would be acceptable placements for a bacterium in non-local
402 dissemination.
403
404 We created two dissemination event probabilities describing local and non-local dissemination.
405 In both, λ is the maximum probability of dissemination and is scaled by a Michaelis-Menten
406 fraction, using a value of CFU at which the probability is half of the maximum value.
407
408 Equation 1 (a) $$Prob_{Local}(t) = \lambda_{Local}\frac{CFU(t)}{CFU(t) + CFU_{half}^{Local}}$$
409 Equation 1 (b) $$Prob_{Nonlocal}(t) = \lambda_{Nonlocal}\frac{CFU(t)}{CFU(t) + CFU_{half}^{Nonlocal}}$$
410
411 ***Granuloma Merging***
412 Experiments demonstrate that a subset of granulomas contain a more than one Mtb barcode (25).
413 Following inoculation or dissemination events, individual granulomas may merge, or are

414 sufficiently close to each other, to form clusters. We identify granuloma clusters and their
415 members when needed for plotting and computing statistics but allow them to evolve
416 independently. Briefly, our algorithm evaluates all intersections of granulomas, and combines
417 groups of granulomas that intersect in 3D space. These grouped granulomas are the granuloma
418 clusters. A granuloma cluster may contain only descendants of a single founder Mtb ID, or may
419 contain descendants of multiple founder Mtb IDs.
420
421 ***Model Parameters, Calibration, and Sensitivity Analysis***
422 We sought to define the parameter space for *MultiGran* across multiple scales. First, we
423 identified the parameter space of the individual granuloma ODE model that best represents the
424 individual granuloma datasets (CFU and cell counts). To determine an initial, wide range of
425 parameter values to test, we examined experimental values from literature, the previous models
426 (37–39), and values from *GranSim*, our single granuloma model that has been calibrated based
427 largely on NHP data (6-17,19-21). We then used a Latin Hypercube Sampling (LHS) algorithm
428 (46) to sample this multi-dimensional parameter space 500 times. This initial wide range of
429 simulations did not match the NHP data. We narrowed the initial ranges and resampled the space
430 in an iterative process until, out of the 500 simulations, ninety percent of the runs fell within the
431 bounds of our experimental data on CFU, T cell counts, and macrophages within individual NHP
432 granulomas. The parameter ranges for these runs are in Table A1.
433
434 Next, we identified the dissemination parameter space of *MultiGran* that matched the NHP
435 whole lung outcome datasets (previously published (20,25,27,31–33) and ongoing studies). We

again utilized LHS to sample this space and identify baseline parameter ranges that match the data (Table A3).

Following *MultiGran* calibration, we sampled the calibrated parameter space to create a biorepository of *in silico* lungs that could be used to make predictions and compare to additional NHP data sets. We then used Partial Rank Correlation Coefficient (PRCC), a global sensitivity analysis technique (46), to identify significant correlations between single granuloma ODE model parameter changes and variation in whole lung outputs. We excluded the dissemination parameters from our multi-scale PRCC analysis because they are phenomenological in nature and we are interested in identifying the mechanistic events that occur at the granuloma scale and lead to dissemination, a whole lung outcome.

Linking Cellular Scale and Tissue Time Scales

We link the cell and cytokine scale events in the ODE model (single granuloma) with the tissue scale ABM (multiple granulomas) to form the multi-scale *MultiGran* model (Figure 2). Linking of timescales is important for proper model design (47). We use an ABM time-step of 1 day. At each ABM time-step, dissemination events can occur. After each ABM time step, the system of ODEs is solved for each granuloma to update the states of all host cells, cytokines and Mtb populations over the next 24 hours. We run the ODEs using adaptive time steps for 1 agent iteration, for each granuloma, before proceeding to the next agent time step, as dissemination events at the agent time step depend on the dynamically-changing state of ODEs. Additionally, the ODE state variable concentrations can be affected by the occurrence of a dissemination event.

459

460 ## Results

461 We present a whole lung model, *MultiGran*, that captures the behavior of Mtb infection leading
462 to the development of multiple granulomas via initial infection and then dissemination of
463 bacteria from existing granulomas. We calibrate and validate the model with unique datasets
464 derived from NHPs, the animal model that most closely mimics the features of human infection.
465 We then use the model to identify dissemination rates and to predict mechanisms leading to
466 dissemination.

467

468 ***Simulated individual granulomas recapitulate in vivo primate granuloma dynamics***

469 We calibrated our single granuloma model, comprised of a system of non-linear ODEs, to data
470 derived from NHP studies. We compared bacterial load (CFU), T cell counts, and macrophage
471 counts over time per granuloma. Our CFU dataset consists of 623 granulomas from 38 NHPs
472 (previously published (20,27,31–33) and ongoing studies). T cell and macrophage counts, as well
473 as additional CFU, were derived from a separate, new dataset of 26 granulomas from 7 Mtb-
474 infected NHPs and baseline data from one uninfected macaque (see Methods). The data from
475 these 7 NHPs capture the timing of the immune system during early events in infection
476 (granulomas from all NHPs were collected between 3-9 weeks post infection) and were
477 imperative for proper calibration of the model.

478

479 We identify a range of parameter values (Table A1) that replicate CFU peaks at approximately
480 35 days and subsequent control of CFU after day 100 post-infection (Figure 3A), macrophage
481 dynamics (Figure 3B), and T-cell dynamics (Figure 3C). These dynamics reflect the initial

inability of the innate immune system to control Mtb replication, the eventual control provided by T cells that arrive from the lymph node around day 28, and the stabilization of Mtb counts around day 100. When isolating a suitable parameter range, we identified ranges that matched these overall trends and recapitulated the spread of granuloma outcomes outlined by the NHP datasets. Likely, our spread captures a fuller range of individual granuloma dynamics than a sample from a limited number of NHP can achieve.

Figure 3: Bacteria, macrophage and T cell dynamics within an individual granuloma. Individual NHP granuloma bacteria **(A)**, macrophages **(B)**, and CD3+ T cells **(C)** shown as orange points across time. Each individual point represents data from a single NHP granuloma. Purple lines indicate simulation outputs from 500 simulations that match NHP data. Light purple shading shows the minimum and maximum of simulation runs, darker purple shading represents the 5^{th} to 95^{th} percentiles of the simulations, and dark purple lines represent the 5^{th}, 50^{th}, and 95^{th} percentiles of simulations. Parameter ranges are listed in Table A1.

MultiGran simulates the appearance of granulomas throughout the lung, as seen in vivo

By employing the calibrated single granuloma model (Figure 3) within our *MultiGran* framework, we can now simulate the spread of infection within the lung. We inoculate with 16 to 21 individual bacteria, mimicking the protocol of Martin et al. (25), placing them within an inoculation region within one of the lower lung lobes, as is done in the NHP inoculations via bronchoscope (see Methods). Each initial granuloma in an NHP arises from a single bacterium in an inoculation event (25). Therefore, we initially establish 16-21 granulomas. A sample simulation at the time-point of 250 days post-infection is shown in Figure 4. The blue lung mesh represents the dataset derived from NHPs for (x,y,z) coordinates of a lung. Placed on this mesh

509 are simulation results – individual granulomas ("agents" in the model) and their location, size,
510 and bacterial origin (barcode). Note that, as in the NHP images of Figure 1, infection is primarily
511 within the inoculation region – but that 7 granulomas disseminated non-locally to the opposite
512 lung. In this simulation, one granuloma cluster was found that contained more than one Mtb
513 barcode, as is shown in the pie chart. Movies of disease progression using this 3D visualization
514 are available on the website http://malthus.micro.med.umich.edu/labmovies/MultiGran/.
515
516
517 **Figure 4: *MultiGran in silico* infection in a non-human primate lung.**
518 A single *in silico* simulation at 250 days post infection from three angles (**A**-anterior view,
519 **B&C**-opposite posterior-lateral views), plotted over a data grid taken from PET/CT images of a
520 single NHP. Granulomas are located within the lung in 3D space. Each circle of a single color
521 represents a granuloma or granuloma cluster with a single Mtb barcode ID. The circle shown as a
522 pie chart represents a granuloma cluster with two unique Mtb barcode IDs; each color represents
523 the relative proportion of CFU of each ID compared to the total CFU of the granuloma cluster,
524 while the overall size of the circle is proportional to the size of the cluster. Inoculation was in the
525 lower right lung (bottom left in each image). Granulomas found in the upper right lung and the
526 left lung result from non-local dissemination within the simulation.
527
528
529
530 ***Simulations are consistent with in vivo infection and predict dissemination likelihood rates***
531 *MultiGran* allows both local and non-local dissemination of bacteria to initiate new granulomas,
532 tracks the origin (Mtb ID) of each granuloma, and allows for merging of nearby granulomas to
533 form a cluster. Each granuloma has a unique parameter set chosen from the ranges in Table A1
534 according to an LHS design. To determine what leads to different dissemination patterns *in vivo*,
535 we use our dataset consisting of four NHPs in that were inoculated with uniquely identifiable
536 Mtb (Figure 1; Martin et al. (25)). Outcome measures from these experiments include: (1) the
537 number of Mtb at time of inoculation (16-21 Mtb), (2) the number of granuloma (or granuloma

clusters) at necropsy (17-28 granulomas), (3) the percentage of Mtb barcodes found in multiple granulomas (12.5 - 68.4%), and (4) the percentage of granulomas containing multiple Mtb barcodes (~10-20%). We calibrated *MultiGran* dissemination dynamics to this dataset by varying the seven dissemination parameters (Table A3). Our whole lung simulations and the NHP dataset are shown in Figure 5. Notice that the simulations capture the full heterogeneity of the *in vivo* results across each NHP. Additionally, the experimental data are from only four NHPs, while our simulations represent a larger, more diverse set of possible outcomes.

Figure 5: *MultiGran* recapitulates non-human primate dissemination outcomes.
Martin et al. (22) infected 4 NHP with 16-21 different Mtb barcodes **(A)**, and after 120 days the NHP immune system formed 16-28 non-sterilized granuloma clusters **(B)**. We replicated these experiments by simulating 200 NHP, which started with 16-21 different Mtb. Of the 16-21 Mtb in NHP, 10%-70% were found in multiple granuloma clusters, meaning at least 10%-70% of Mtb were disseminating. Similar to the NHP data, our simulations have 0%-90% of Mtb barcodes disseminated to multiple granuloma clusters **(C)**. Within the NHP experiments, of the 16-28 non-sterilized granuloma clusters, 10%-25% had multiple Mtb IDs within them, meaning at least 10%-25% of observed granulomas are clusters involving multiple sources of Mtb infection. Our 200 MultiGran simulations demonstrate a similar range of granuloma clusters with multiple Mtb barcodes **(D)**. Simulations are shown in gray whereas NHP experiment outcomes are shown in blue. Each point represents a single NHP or *in silico* simulated granuloma.

To more directly test for non-local dissemination events, we validate our simulations against a second dataset of 38 NHPs (Figure 6). Within this NHP dataset, we identified the lung that contained the most granulomas for each NHP, and termed this lung the more-populated lung. Next, we calculated the percentage of granulomas that resided in the more-populated lung out of the total number of granulomas across both lungs. We found that the 38 NHPs exhibited a range of 52%-100% of granulomas in the lung that was more-populated. Results from the same

simulations used to create Figure 5 give a range ~54%-100%, providing additional support for the model in its ability to capture the range of data offered by NHP experiments.

Figure 6: MultiGran recapitulates spread of infection data.
At necropsy of 38 NHP experiments, we identified the lung that contained the most granulomas for each NHP. Next, we calculated the percentage of granulomas that resided in the more-populated lung out of the total number of granulomas. We found that 52-100% of granulomas formed resided within the more-populated lung. Blue dots represent each NHP experiment. We ran 200 *in silico* simulations that capture a similar range to the NHP spread of infection from lung to lung, ranging from 54.3% to 100%. Gray dots represent each simulated lung.

When examining *in vivo* data, the total number of dissemination events may be undercounted due to sterilization and granuloma clustering. In contrast, our model is able to count every dissemination event, and thereby provides a predicted frequency of local and non-local dissemination. We found that, on average, the rate of dissemination is about 1/24 dissemination events per granuloma per month for simulations run out to 250 days. Most dissemination occurs earlier in the infection, as noted in Martin, et al. (25). Further, *MultiGran* predicts that local dissemination events occur about twice as frequently as non-local dissemination events.

MultiGran simulations match individual NHP infections

From our repository of 200 *MultiGran* simulated lungs, we isolated the five simulations that yielded the closest match to the median values of Mtb inoculation (20), the median number of granulomas at necropsy (20.5), the median percentage of Mtb barcodes that were found in

multiple granulomas (14.3%), and the median percentage of granulomas that contained multiple Mtb barcodes (17.5%) across the four NHP from Martin et al. (25).

These five simulations represent the best matches to the NHP used in Martin et al. (25). We compare two of these simulations to the CFU/granuloma at necropsy from NHP:179-14 (Figure 7A & 7C). Both lung simulations display satisfactory matches to the NHP CFU data; both simulations cover the spread of the experimental data while lying within the bounds of the dataset. However, while both simulations match the CFU data at 17 weeks, we are able to predict what could have happened beyond the necropsy date by running the simulation for a longer time period. Shown are two distinct possible outcomes with the same parameter set: note they diverge when predicting later dissemination events. Figure 7B shows one simulation predicts bacterial control across all the granulomas within that simulation. Figure 7D shows another outcome. Here, a single granuloma within the lung exhibits uncontrolled bacterial growth leading to dissemination and there is also formation of new granulomas via both local and non-local dissemination (at days 145, 166, and 193). These simulations suggest that NHP:179-14 was either containing the bacteria (i.e., LTBI) (our prediction in Figure 7B) or could have had a subclinical infection that was on the edge of leading to multiple dissemination events (our prediction in Figure 7D). Simulations that match the other NHP are not shown, but show similar trends and predictions.

Figure 7: **MultiGran matches individual NHP granuloma dynamics and predicts CFU burden across time.**
We compared the CFU/granuloma at necropsy for NHP:179-14 **(A&C)** to two separate simulations that matched these outcomes. Blue dots represent single granuloma values taken

618 from NHP:179-14; gray dots represent simulation values at comparable timepoints. Simulation
619 predictions diverged after 17 weeks. One simulation predicted stability – i.e., granuloma
620 containment of bacteria **(B)**. The other simulation **(D)** predicted uncontrolled growth of bacteria
621 within one granuloma, leading to dissemination and the formation of other granulomas across
622 time. Each line in **(B&D)** represents one granuloma realization within *MultiGran* across time.
623 Blue dots represent NHP:179 granuloma CFU values. Simulation behavior to the right of the
624 blue dots should be considered a prediction.
625

626

627 ***Sensitivity analysis reveals important mechanisms responsible for dissemination***

628 To predict the mechanisms that lead to dissemination events within lungs, we perform global
629 sensitivity analysis on four whole lung outcomes of interest: the number of dissemination events,
630 the total number of granuloma clusters at the end of the simulation, the percentage of granuloma
631 clusters that contain multiple barcodes, and the percentage of granulomas that occupy the
632 initially-inoculated lung at the end of the simulation. We quantify the contributions of each
633 model parameter to the outcomes of interest by calculating partial rank correlation coefficients
634 (PRCC) at the end of the simulation (250 days). Our analysis reveals one parameter as the main
635 driver of these four whole lung outcomes (Table 1). Parameter *CD8MultiFunc* describes the
636 multi-functional nature of CD8+T cells, i.e., the amount of overlap of cytotoxic function and
637 cytokine expression in CD8+ T cells, and is significantly correlated with each of the four
638 outcomes. If *CD8MultiFunc* is increased so that a greater proportion of CD8+ T cells exhibits
639 multi-functionality, then a larger percentage of granulomas will reside within a single lung (less
640 non-local dissemination) and there will be fewer dissemination events and fewer granulomas
641 overall. CD8+ T cells are a key host cell in a functional immune response to Mtb infection, and if
642 the subpopulation that can perform multiple roles within the complex microenvironment of a
643 granuloma increased, it would certainly benefit the host.
644

Parameter Name	Parameter Description	Number of Dissemination Events	Granulomas at End of Simulation	Granulomas with Multiple Barcodes	Granulomas in Dominant Lung
CD8MultiFunc	overlap of cytotoxic function and cytokine expression in CD8+ T cells	-0.39	-0.38	-0.14	0.32

Table 1: CD8+ T cell functionality plays an important role in dissemination outcomes. PRCCs are shown for parameter *CD8MultiFunc*, the overlap of cytotoxic function and cytokine expression in CD8+ T cells is significantly correlated with each of the four whole lung outcomes at the end of the simulation (200 days). Parameter *CD8MultiFunc* is negatively correlated with the total number of dissemination events across the simulation, the number of granulomas present at the end of the simulation, and the percentage of granulomas that contain multiple barcodes. It is positively correlated with the percentage of granulomas that reside in the more-populated lung.

If we exclude parameter *CD8MultiFun* from the analysis, we reveal secondary contributions of other parameters to the whole lung outcomes (Table 2). Notably, the role of macrophage-bacteria interactions is found to be important. *k18* represents the base rate of killing of extracellular bacteria by macrophages. If this rate is high, there are fewer dissemination events and fewer granulomas across the simulation. Additionally, *k17* represents the maximum bursting rate of infected macrophages. This parameter is positively correlated with the number of dissemination events and the number of granulomas across a simulation. If bursting occurs at a high rate within a granuloma, our model predicts that a granuloma is more likely to disseminate both locally and non-locally. Taken together, these two parameters identify an important role for macrophage dynamics within the granuloma: if macrophages cannot adequately respond to Mtb, the likelihood of dissemination increases. Altogether, the results of this analysis represent a multi-scale impact: events governing cell function at the cellular scale impact local and non-local

669 dissemination outcomes across the lungs and predict the difference between dissemination and
670 control across the lung environment.
671

Parameter Name	Parameter Description	Number of Dissemination Events	Number of Granulomas and Clusters	Percentage of Granulomas with Multiple Barcodes	Percentage of Granulomas in More-Populated Lung
k18	Extracellular bacteria killed by macrophages	-0.11	-0.11	-0.041	0.11
nuI10	decay rate of IL-10 cytokine	-0.088	-0.087	-0.068	0.089
Sr1b	TNF based recruitment of primed CD4+ T cells	-0.075	-0.074	-0.044	0.06
k6	rate of differentiation from primed to Th1 CD4+ T cells	-0.084	-0.073	-0.047	0.071
s12	cell production of IL-12	-0.058	-0.056	-0.025	0.056
w	contribution of intracellular bacteria to resting macrophage activation	-0.037	-0.04	-0.021	0.04
s2	half-saturation of IL-4	-0.024	-0.021	-0.025	0.02
Sr3b	TNF based recruitment of Th2 CD4+ T cells	-0.036	-0.033	-0.021	0.025
alpha30	TNF production by infected macrophages	0.032	0.028	0.022	-0.037
nuTg	IFNg induced apoptosis of Th1 CD4+ T cells	0.057	0.055	0.037	-0.04
s4b	half-saturation of TNF on local resting macrophage recruitment	0.042	0.043	0.04	-0.043
k17	max rate of infected macrophages bursting	0.14	0.14	0.076	-0.12

672

673 **Table 2: Sensitivity Analysis reveals global drivers of dissemination outcomes.**
674 Excluding parameter *CD8MultiFunc*, 12 parameters were identified as having a significant
675 impact on each of 4 *MultiGran* whole lung simulation outcomes at the end of the simulation. All
676 PRCCs shown are significant to $p < .05$.
677

678

679 ## Discussion

Tuberculosis is a complex and heterogeneous disease with a spectrum of outcomes, and the myriad of mechanisms that influence outcomes of initial infection are poorly defined. Our data in NHP models, and bolstered by data in humans, support the notion that each individual granuloma in a host is independent and dynamic, in terms of immunologic composition and function, ability to kill or restrain Mtb bacilli, and risk for dissemination or reactivation (48,49). However, it can be challenging in NHP models to determine the full range of host mechanisms that play a role in initial containment and prevention of dissemination, both of which are essential to limiting development of active TB. In the pursuit of a better understanding of the collective behavior of lung granulomas in individuals infected with Mtb, we performed a systems biology approach pairing NHP experiments and computational/mathematical modeling. Specifically, we explored events that lead to dissemination and new granuloma formation, and several studies have recently explored this biological phenomenon (25,36,50,51). In particular, the barcoding technique introduced by Martin et al. showed that dissemination varies widely among macaques despite initial infection conditions being similar, and that in individual macaques, each granuloma had a different dissemination risk, from no dissemination by most granulomas, even though these granulomas were CFU+, to multiple dissemination events from a single granuloma. The barcoding analysis provided critical new information about bacterial spread within the lung. However, identifying mechanisms that leading to granuloma dissemination, which is linked to development of active TB (36), is important in designing more effective vaccines and therapeutics against TB. Systems biology approaches can address these mechanisms and more generally contribute to our still limited understanding of Mtb infection dynamics.

In this work, we combine experimental data from NHPs with a novel multi-scale, hybrid agent-based model of granuloma formation, function and dissemination within the lung, called *MultiGran*. We calibrate and validate *MultiGran* against multiple NHP datasets that span cellular, bacterial, granuloma, and whole-lung scales. This calibration and validation allowed us to make predictions about dissemination within Mtb infected lungs. We report that the likelihood of local dissemination is approximately two times greater than non-local dissemination, which supports the in vivo data reported in Martin, et al. (25), and we used sensitivity analysis techniques to identify that dissemination is intertwined with the role of CD8+ T cells in granulomas. Specifically, we predict that the functionality of CD8+ T cells is critically important: if a greater percentage of CD8+ T cells can perform dual functions of cytokine expression (IFNγ, TNF, and IL-10) and cytotoxicity, then the likelihood of dissemination significantly decreases.

The role of CD8+ T cell multi-functionality within the granuloma is controversial (for reviews of CD8+ T cells in TB, see (52,53), (20)). While the majority of T cells within a granuloma are single cytokine producers (27), multifunctional CD8+ T cells have been demonstrated in the blood of Mtb-infected humans and the proliferation and response rate of these cells differed between active and latent infection (54,55). Together, these studies and our current work suggest a need for increased focus on this specific cell type to evaluate the potential that CD8+ multifunctional T cells may offer.

The NHP datasets generated within this study are unique and critical to the predictions of *MultiGran*. In addition, these data also present new insights into early events occurring during

Mtb infection. In particular, the ability to capture data on Mtb infection during early time points for CFU, T cell counts, and macrophage numbers is instrumental in elaborating timing of early immune response events. These early events in primates have been understudied, and knowledge of the role that timing plays in granuloma establishment, formation, and development is critical to early intervention strategies.

Using *MultiGran*, we were able to match to granuloma population data coming from multiple monkeys (Figure 5 & 6) and granulomas (Figure 3). we were also able to match experimental data from a single NHP (Figure 7). In the era of precision medicine (56), the ability of *MultiGran* to fit to individual data could help predict, in real time, whether the granulomas within that individual are likely to disseminate. This could happen when paired with PET/CT images of individually lung granulomas. However, more realistically, this provides an impetus for identifying biomarkers that are associated with granulomas at risk of dissemination, which could be more widely used to identify persons at risk of developing active TB following infection.

There are a few limitations of our study and model. First, the driving dissemination probability rules are somewhat phenomenological. Our goal in this first study was to rely on as few assumptions as possible; the only granuloma characteristic that is explicitly used in the dissemination rules is the total bacterial burden. As a consequence, the model allows for even a stable, mature granuloma to disseminate (with small probability). We addressed this by allowing T cells to leave the parent granuloma to travel to a daughter granuloma in a local dissemination event, expecting this to sterilize new granulomas. Surprisingly, this was largely ineffective. Instead, it is more likely that the lung parenchyma in infected individuals has increased numbers

748 of Mtb specific T cells and possibly activated macrophages, so that new granulomas form in a
749 completely different immune environment, compared to the initial granulomas that form in an
750 immunologically naïve environment. This notion is supported by our data in NHP models
751 demonstrating that primary ongoing infection protects against reinfection (32). *MultiGran* could
752 be refined to test this in future iterations. Second, we restrict dissemination to be within the
753 boundary of the lungs, but the actual environment within the lungs is very complicated and also
754 could include airways and blood. Third, while we acknowledge thoracic lymph nodes as a source
755 of non-local dissemination, and include adaptive immune cell recruitment in our ODE model, we
756 currently do not explicitly model lymph node compartments. In future work, we plan to address
757 the role of lymph nodes in Mtb infection and dissemination. Finally, while *MultiGran* was
758 developed based on extensive NHP and human data, it does not contain all the various cell types
759 and mechanisms in the complex environment of the granuloma, primarily because the functions
760 and importance of certain cell types and factors remain obscure. As data become available,
761 *MultiGran* can evolve to include additional factors for mechanistic test.
762
763 In summary, we utilized a systems biology approach that combined computational modeling and
764 NHP datasets to better understand mechanisms of granuloma dissemination. We present
765 *MultiGran*, the first multi-scale model of granuloma dissemination and formation, that was
766 calibrated and validated to NHP data and we make predictions about the rate of dissemination
767 and the role of specific immune cells in granuloma dissemination. In particular, we discovered
768 roles for multifunctional CD8+ T cells and macrophage dynamics in preventing local and non-
769 local dissemination within the lungs. Altogether, we argue that *MultiGran*, together with NHP

770 experimental approaches, offers great potential to understand and predict dissemination events
771 within Mtb infected lungs.
772

773 Acknowledgments

774 This research was supported by R01AI123093 awarded to DEK and JLF; R01HL110811
775 awarded to DEK, JLF, and JLL; and UO1HL131072 awarded to DEK, JLF, and JLL.
776 Simulations also use resources of the National Energy Research Scientific Computing Center,
777 which is supported by the Office of Science of the U.S. Department of Energy under Contract
778 No. ACI-1053575 and the Extreme Science and Engineering Discovery Environment (XSEDE),
779 which is supported by National Science Foundation grant MCB140228. We thank Paul Wolberg
780 for programming assistance. We thank the members of the Flynn lab, especially Nicole Grant,
781 Amy Myers, Mark Rodgers, Jaime Tomko, L. Jim Frye, Brianne Stein, Chelsea Causgrove,
782 Carolyn Bigbee, Pauline Maiello, Alexander White, and Cassaundra Ameel for technical
783 assistance, as well as Dr. Philana Ling Lin and Dr. Charles Scanga for advice and assistance.
784
785
786
787

788 References

789

790 1. WHO. WHO Global tuberculosis report 2016 [Internet]. World Health Organization Press.
791 2016. Available from: http://www.who.int/tb/publications/global_report/en/
792 2. Houben RMGJ, Esmail H, Emery JC, Joslyn LR, McQuaid CF, Menzies NA, et al.

Spotting the old foe—revisiting the case definition for TB. Lancet Respir Med [Internet]. 2019;7(3):199–201. Available from: https://linkinghub.elsevier.com/retrieve/pii/S2213260019300384

3. Lin PL, Ford CB, Coleman MT, Myers AJ, Gawande R, Ioerger T, et al. Sterilization of granulomas is common in active and latent tuberculosis despite within-host variability in bacterial killing. Nat Med. 2014;20(1):75–9.

4. Gideon HP, Flynn JL. Latent tuberculosis: What the host "sees"? Immunol Res. 2011;50(2–3):202–12.

5. Lin PL, Myers A, Smith L, Bigbee C, Bigbee M, Fuhrman C, et al. Tumor necrosis factor neutralization results in disseminated disease in acute and latent Mycobacterium tuberculosis infection with normal granuloma structure in a cynomolgus macaque model. Arthritis Rheum. 2010;62(2):340–50.

6. Diedrich CR, Mattila JT, Klein E, Janssen C, Phuah J, Sturgeon TJ, et al. Reactivation of latent tuberculosis in cynomolgus macaques infected with SIV is associated with early peripheral T cell depletion and not virus load. PLoS One. 2010;5(3).

7. Mattila JT, Diedrich CR, Lin PL, Phuah J, Flynn JL. Simian Immunodeficiency Virus-Induced Changes in T Cell Cytokine Responses in Cynomolgus Macaques with Latent Mycobacterium tuberculosis Infection Are Associated with Timing of Reactivation . J Immunol. 2011;186(6):3527–37.

8. Chen CY, Huang D, Wang RC, Shen L, Zeng G, Yao S, et al. A critical role for CD8 T cells in a nonhuman primate model of tuberculosis. PLoS Pathog. 2009;5(4).

9. Sershen CL, Plimpton SJ, May EE. Oxygen Modulates the Effectiveness of Granuloma Mediated Host Response to Mycobacterium tuberculosis: A Multiscale Computational

816 Biology Approach. Front Cell Infect Microbiol. 2016;

817 10. Gough M, May E. An in silico model of the effects of Vitamin D3 on mycobacterium
818 infected macrophage. In: Proceedings of the Annual International Conference of the IEEE
819 Engineering in Medicine and Biology Society, EMBS. 2016.

820 11. Linderman JJ, Kirschner DE. In silico models of M. Tuberculosis infection provide a route
821 to new therapies. Drug Discov Today Dis Model. 2015;15:37–41.

822 12. Kirschner D, Pienaar E, Marino S, Linderman JJ. A review of computational and
823 mathematical modeling contributions to our understanding of Mycobacterium tuberculosis
824 within-host infection and treatment. Curr Opin Syst Biol [Internet]. 2017;3:170–85.
825 Available from: http://linkinghub.elsevier.com/retrieve/pii/S2452310016300117

826 13. Hao W, Schlesinger LS, Friedman A. Modeling granulomas in response to infection in the
827 lung. PLoS One. 2016;11(3).

828 14. Warsinske HC, Pienaar E, Linderman JJ, Mattila JT, Kirschner DE. Deletion of TGF-β1
829 increases bacterial clearance by cytotoxic t cells in a tuberculosis granuloma model. Front
830 Immunol. 2017;8(DEC).

831 15. Linderman JJ, Cilfone NA, Pienaar E, Gong C, Kirschner DE. A multi-scale approach to
832 designing therapeutics for tuberculosis. Integr Biol (United Kingdom) [Internet].
833 2015;7(5):591–609. Available from: http://xlink.rsc.org/?DOI=C4IB00295D

834 16. Cilfone NA, Perry CR, Kirschner DE, Linderman JJ. Multi-Scale Modeling Predicts a
835 Balance of Tumor Necrosis Factor-α and Interleukin-10 Controls the Granuloma
836 Environment during Mycobacterium tuberculosis Infection. PLoS One. 2013;8(7).

837 17. Fallahi-Sichani M, Kirschner DE, Linderman JJ. NF-??B signaling dynamics play a key
838 role in infection control in tuberculosis. Front Physiol. 2012;3 JUN.

18. Prats C, Vilaplana C, Valls J, Marzo E, Cardona PJ, López D. Local inflammation, dissemination and coalescence of lesions are key for the progression toward active tuberculosis: The bubble model. Front Microbiol. 2016;7(FEB).

19. Marino S, Linderman JJ, Kirschner DE. A multifaceted approach to modeling the immune response in tuberculosis. Wiley Interdiscip Rev Syst Biol Med. 2011;3(4):479–89.

20. Marino S, Gideon HP, Gong C, Mankad S, McCrone JT, Lin PL, et al. Computational and Empirical Studies Predict Mycobacterium tuberculosis-Specific T Cells as a Biomarker for Infection Outcome. PLoS Comput Biol. 2016;12(4).

21. Flynn JL, Tsenova L, Izzo A, Kaplan G. Experimental Animal Models of Tuberculosis. In: Handbook of Tuberculosis. 2017. p. 389–426.

22. Wong EA, Joslyn L, Grant NL, Klein E, Lin PL, Kirschner DE, et al. Low Levels of T Cell Exhaustion in Tuberculous Lung Granulomas. Infect Immun. 2018;86(9).

23. Pienaar E, Linderman JJ, Kirschner DE. Emergence and selection of isoniazid and rifampin resistance in tuberculosis granulomas. PLoS One. 2018;13(5).

24. Sarathy J, Blanc L, Alvarez-Cabrera N, O'Brien P, Dias-Freedman I, Mina M, et al. Fluoroquinolone Efficacy against Tuberculosis Is Driven by Penetration into Lesions and Activity against Resident Bacterial Populations. Antimicrob Agents Chemother. 2019;63(5).

25. Martin CJ, Cadena AM, Leung VW, Lin PL, Maiello P, Hicks N, et al. Digitally Barcoding Mycobacterium tuberculosis Reveals In Vivo Infection Dynamics in the Macaque Model of Tuberculosis . MBio. 2017;8(3).

26. Flynn JL, Gideon HP, Mattila JT, Lin P ling. Immunology studies in non-human primate models of tuberculosis. Immunol Rev. 2015;264(1):60–73.

862 27. Gideon HP, Phuah JY, Myers AJ, Bryson BD, Rodgers MA, Coleman MT, et al.
863 Variability in Tuberculosis Granuloma T Cell Responses Exists, but a Balance of Pro- and
864 Anti-inflammatory Cytokines Is Associated with Sterilization. PLoS Pathog.
865 2015;11(1):1–28.
866 28. Lin PL, Rodgers M, Smith L, Bigbee M, Myers A, Bigbee C, et al. Quantitative
867 comparison of active and latent tuberculosis in the cynomolgus macaque model. Infect
868 Immun. 2009;77(10):4631–42.
869 29. Lin PL, Pawar S, Myers A, Pegu A, Fuhrman C, Reinhart TA, et al. Early events in
870 Mycobacterium tuberculosis infection in cynomolgus macaques. Infect Immun. 2006;
871 30. Lin PL, Coleman T, Carney JPJ, Lopresti BJ, Tomko J, Fillmore D, et al. Radiologic
872 Responses in Cynomolgus Macaques for Assessing Tuberculosis Chemotherapy
873 Regimens. Antimicrob Agents Chemother [Internet]. 2013 Sep 15;57(9):4237–44.
874 Available from: http://www.ncbi.nlm.nih.gov/pmc/articles/PMC3754323/
875 31. Phuah J, Lin PL, Flynn JL, Chan J, Hendricks MR, Maiello P, et al. Effects of B Cell
876 Depletion on Early Mycobacterium tuberculosis Infection in Cynomolgus Macaques.
877 Infect Immun. 2016;84(5):1301–11.
878 32. Cadena AM, Hopkins FF, Maiello P, Carey AF, Wong EA, Martin CJ, et al. Concurrent
879 infection with Mycobacterium tuberculosis confers robust protection against secondary
880 infection in macaques. PLoS Pathog. 2018;14(10).
881 33. Darrah PA, DiFazio RM, Maiello P, Gideon HP, Myers AJ, Rodgers MA, et al. Boosting
882 BCG with proteins or rAd5 does not enhance protection against tuberculosis in rhesus
883 macaques. npj Vaccines. 2019;4(1).
884 34. van der Walt S, Schönberger JL, Nunez-Iglesias J, Boulogne F, Warner JD, Yager N, et al.

885 scikit-image: image processing in Python. PeerJ. 2014;2:e453.

886 35. Wiktorski T. Spark. Adv Inf Knowl Process. 2019;85–97.

887 36. Coleman MT, Maiello P, Tomko J, Frye LJ, Fillmore D, Janssen C, et al. Early changes
888 by 18Fluorodeoxyglucose positron emission tomography coregistered with computed
889 tomography predict outcome after Mycobacterium tuberculosis infection in cynomolgus
890 macaques. Infect Immun. 2014;82(6):2400–4.

891 37. Wigginton JE, Kirschner D. A Model to Predict Cell-Mediated Immune Regulatory
892 Mechanisms During Human Infection with Mycobacterium tuberculosis. J Immunol.
893 2001;166(3):1951–67.

894 38. Sud D, Bigbee C, Flynn JL, Kirschner DE. Contribution of CD8+ T Cells to Control of
895 Mycobacterium tuberculosis Infection. J Immunol. 2014;176(7):4296–314.

896 39. Guzzetta G, Kirschner D. The Roles of Immune Memory and Aging in Protective
897 Immunity and Endogenous Reactivation of Tuberculosis. PLoS One. 2013;8(4).

898 40. Cilfone NA, Ford CB, Marino S, Mattila JT, Gideon HP, Flynn JL, et al. Computational
899 Modeling Predicts IL-10 Control of Lesion Sterilization by Balancing Early Host
900 Immunity–Mediated Antimicrobial Responses with Caseation during Mycobacterium
901 tuberculosis Infection. J Immunol. 2015;194(2):664–77.

902 41. Marino S, Myers A, Flynn JL, Kirschner DE. TNF and IL-10 are major factors in
903 modulation of the phagocytic cell environment in lung and lymph node in tuberculosis: A
904 next-generation two-compartmental model. J Theor Biol. 2010;265(4):586–98.

905 42. Redford PS, Murray PJ, O'Garra A. The role of IL-10 in immune regulation during M.
906 tuberculosis infection. Mucosal Immunol. 2011;4(3):261–70.

907 43. Mahamed D, Boulle M, Ganga Y, Mc Arthur C, Skroch S, Oom L, et al. Intracellular

growth of Mycobacterium tuberculosis after macrophage cell death leads to serial killing of host cells. Elife. 2017;6.

44. Huang L, Nazarova E V., Tan S, Liu Y, Russell DG. Growth of Mycobacterium tuberculosis in vivo segregates with host macrophage metabolism and ontogeny . J Exp Med. 2018;215(4):1135–52.

45. Hoal-Van Helden EG, Hon D, Lewis LA, Beyers N, Van Helden PD. Mycobacterial growth in human macrophages: Variation according to donor, inoculum and bacterial strain. Cell Biol Int. 2001;25(1):71–81.

46. Marino S, Hogue IB, Ray CJ, Kirschner DE. A methodology for performing global uncertainty and sensitivity analysis in systems biology. Vol. 254, Journal of Theoretical Biology. 2008. p. 178–96.

47. Cilfone NA, Kirschner DE, Linderman JJ. Strategies for Efficient Numerical Implementation of Hybrid Multi-scale Agent-Based Models to Describe Biological Systems. Vol. 8, Cellular and Molecular Bioengineering. 2015. p. 119–36.

48. Cadena AM, Fortune SM, Flynn JL. Heterogeneity in tuberculosis. Nat Rev Immunol. 2017;17(11):691–702.

49. Cadena AM, Flynn JL, Fortune SM. The importance of first impressions: Early events in mycobacterium tuberculosis infection influence outcome. Vol. 7, mBio. 2016.

50. Lin PL, Maiello P, Gideon HP, Coleman MT, Cadena AM, Rodgers MA, et al. PET CT Identifies Reactivation Risk in Cynomolgus Macaques with Latent M. tuberculosis. PLoS Pathog [Internet]. 2016 Jul 5;12(7):e1005739. Available from: https://doi.org/10.1371/journal.ppat.1005739

51. Maiello P, DiFazio RM, Cadena AM, Rodgers MA, Lin PL, Scanga CA, et al. Rhesus

macaques are more susceptible to progressive tuberculosis than cynomolgus macaques: A quantitative comparison. Infect Immun. 2018;86(2).

52. Lin PL, Flynn JL. CD8 T cells and Mycobacterium tuberculosis infection. Semin Immunopathol [Internet]. 2015;37(3):239–49. Available from: http://link.springer.com/10.1007/s00281-015-0490-8

53. Prezzemolo T, Guggino G, La Manna MP, Di Liberto D Di, Dieli F, Caccamo N. Functional signatures of human CD4 and CD8 T cell responses to Mycobacterium tuberculosis. Vol. 5, Frontiers in Immunology. 2014.

54. Rozot V, Vigano S, Mazza-Stalder J, Idrizi E, Day CL, Perreau M, et al. Mycobacterium tuberculosis-specific CD8+ T cells are functionally and phenotypically different between latent infection and active disease. Eur J Immunol. 2013;43(6):1568–77.

55. Commandeur S, Lin MY, van Meijgaarden KE, Friggen AH, Franken KLMC, Drijfhout JW, et al. Double- and monofunctional CD4 + and CD8 + T-cell responses to Mycobacterium tuberculosis DosR antigens and peptides in long-term latently infected individuals. Eur J Immunol. 2011;41(10):2925–36.

56. Collins FS, Varmus H. A new initiative on precision medicine. N Engl J Med [Internet]. 2015;372(9):793–5. Available from: http://www.ncbi.nlm.nih.gov/pubmed/25635347%0Ahttp://www.pubmedcentral.nih.gov/articlerender.fcgi?artid=PMC5101938

Appendix 1 (Equations pdf that is attached)

Appendix 2

Parameter name	Min	Max	Units	Ref	Description
Srm	0	0	1/day	fit	MR recruitment rate
alpha4a	0.57	0.83	1/day	(38), (39), fit	Macrophage recruitment of MR
w	0.29	0.33	--	(37), (39), fit	Contribution of BI to MR activation
w3	0.23	0.37	--	(38), (39), fit	Max contribution of Th1 to MI apoptosis
w2	1	1	--	(37), (39), fit	Contribution of MI to MR recruitment
Sr4b	650	750	1/day	(38), (39), fit	Falpha-dependent recruitment of MR
f8	0.002	0.002	--	fit	Ratio adjustment IL-10/Falpha on MR recruitment
f9	0.6	0.6	--	fit	Ratio adjustment Falpha/IL-10
s4b	3210	4860	pg/ml	(57), (39), fit	Half saturation of Falpha on MR recruitment
s4b1	6780	9410	pg/ml	(38), (39), fit	Half saturation of Falpha dependent Th1 recruitment
s4b2	5340	9420	pg/ml	(57), (39), fit	Half saturation of Falpha-dependent T0 recruitment
k4	0.074	0.17	1/day	(37), (39), fit	MA deactivation by IL-10
s8	200	940	pg/ml	(37), (39), fit	Half saturation of IL-10 on MA deactivation
k2	0.43	2.2	1/day	(37), (39), fit	MR infection rate
c9	1190	7450	count	(37), (39), fit	Half saturation of BE on MR infection
k3	0.04	0.04	1/day	(37), (39), fit	MR activation rate
f1	150	150	--	(37), (39), fit	Adjustment IL-4/IFNg
s1	54	450	pg/ml	(37), (39), fit	Half saturation of IFNg-dependent MR activation
Beta	1.00E+07	1.00E+07	1/pg	(38), (39), fit	Scaling factor of Falpha for MR activation
c8	175370	363170	count	fit	Half saturation of BE and BI on MR activation
nuMR	0.005	0.005	1/day	(37), (39), fit	MR death rate
k17	0.1	0.3	1/day	(37), (39), fit	Max rate of MI bursting
N	20	25	count	(37), (39), (40), fit	Carrying capacity of MI
k14a	0.06	0.34	1/day	(38), (39), fit	T cell induced apoptosis of MI
c4	400	880	--	(37), (39), fit	Half saturation of Th1/MI ratio on MI apoptosis
k14b	0.63	0.86	1/day	(38), (39), fit	Falpha induced apoptosis of MI
k52	0.6	0.7	1/day	(38), (39)	Cytotoxic killing of MI
w1	0.2	0.7	--	(38), (39), fit	Max contribution of Th1 to cytotoxic killing
c52	103290	246770	--	fit	Half saturation of TC on MI killing
cT1	35	35	--	fit	Half saturation of Th1 on cytotoxic killing
nuMI	0.0033	0.0033	1/day	(37), (39), (40)	MI death rate
nuMA	0.17	0.17	1/day	(37), (39), fit	MA death rate
alpha1a	0.03	0.55	1/day	(58), (39), fit	Macrophage recruitment of T0
Sr1b	2E+04	5E+4	1/day	(58), (39), fit	Falpha dependent T0 recruitment
alpha2	0.12	0.36	1/day	(37), (39), fit	Max growth rate of T0
c15	2.75E+06	4.09E+06	--	(37), (39), fit	Half saturation of MA on IFNg production by Th1
k6	0.1	0.2	ml/(pg day)	(37), (39), fit	Max T0 to Th1 rate
f7	7	30	--	(38), (39), fit	Effect of IL-10 on IFNg induced differentiation of T0 to Th1
k7	0.25	0.64	ml/(pg day)	(37), (39), fit	Max T0 to Th2 rate
f2	0.2	0.4	--	fit	Adjustment IFNg/IL-4

s2	400	900	pg/day	fit	Half saturation IL-4
nuT0	0.22	0.22	1/day	(37), (39), fit	T0 death rate
CD8MultiFunc	0.7	0.9	--	(38), (39), fit	overlap between TC and T8 function
alpha3a	0.4	0.8	1/day	fit	Macrophage recruitment of Th1
Sr3b	15	80	1/day	Fit	Falpha dependent recruitment of Th2
alpha3a2	0.22	0.75	1/day	fit	Macrophage recruitment of Th2
Sr3b2	50	90	1/day	fit	Falpha dependent recruitment of Th2
nuTg	0.24	0.75	1/day	fit	IFNg induced apoptosis of Th1
c	270	690	pg/ml	fit	Half saturation IFNg on Th1 apoptosis
nuT1	0.33	0.33	1/day	(37), (39)	Th1 death rate
nuT2	0.33	0.33	1/day	(37), (39)	Th2 death rate
alpha3ac	0.25	0.77	1/day	fit	Macrophage recruitment of TC and T8
Sr3bc	14	26	1/day	fit	Falpha dependent recruitment of TC and T8
nuTCg	0.45	0.83	1/day	fit	IFNg induced apoptosis of TC and T8
cc	350	590	pg/ml	(59), (39), fit	Half saturation of IL on TC and T8 apoptosis
nuTC	0.3	0.3	1/day	(38)	TC death rate
sg	2375	7340	pg/(ml day)	fit	IFNg production by cells
c10	5.50E+05	6.35E+06	count	(37), (39), fit	Half saturation of Mtb on IFNg production by cells
s7	590	820	pg/ml	fit	Half saturation of IL-12 on IFNg production by cells
alpha5a	0.6	0.8	pg/day	(38), (39), fit	IFNg production by Th1
c5a	315	630	1/ml	fit	Half saturation of MA on IFNg production by Th1
alpha5b	0.15	0.58	pg/day	(38), (39), fit	IFNg production by T8
alpha5c	0.08	0.35	pg/ml	(38), (39), fit	IFNg production by MI
c5b	160	795	count	fit	Half saturation of MA on IFNg production by T8
alpha7	0.012	0.16	pg/ml	(37), (39), fit	IFNg production by T0
f4	1.5	1.5	--	(37), (39), fit	Adjustment of IL-10/IL-12 on IFNg
s4	270	890	pg/ml	(37), (39), fit	Half saturation of IL-12 on IFNg
nuIG	6	9	1/day	(37), (39), fit	IFNg decay rate
alpha23	0.004	0.004	pg/ml	(38), (39), fit	IL-12 production by MR
c23	140	525	1/ml	(38), (39), fit	Half saturation of Mtb on IL-12 production by MR
alpha8	0.38	0.80	pg/day	(37), (39), fit	IL-12 Production by MA
s12	2330	3650	pg/(ml day)	(38), (39), fit	Cell production of IL-12
c230	390	710	count	Fit	Half saturation of Mtb on IL-12 production by DC's
nuIL-12	1.1	1.1	1/day	(37)	IL-12 death rate
s	170	650	pg/ml	fit	IL-10 effect on IL-12 production by MA
s6	680	770	pg/ml	Fit	Half saturation of IL-10 self-inhibition in MA
f6	0.35	0.35	--	(37)	Adjustment IFNg on IL-10
delta7	0.40	0.8	pg/ml	fit	IL-10 production by MA
alpha16	0.33	0.8	pg/day	Fit, (40)	IL-10 production by Th1
alpha17	0.3	0.5	pg/day	Fit, (40)	IL-10 production by Th2
alpha18	0.5	0.7	pg/day	Fit, (40)	IL-10 production by TC and T8
nuIL-10	1.81	4.1	1/day	(37), fit	IL-10 decay rate
alpha11	0.0033	0.073	pg/day	(37), fit	IL-4 production by T0
alpha12	0.02	0.06	pg/day	(37), fit	IL-4 production by Th2
nuIL-4	2.7	2.7	1/day	(37)	IL-4 decay rate

alpha30	0.05	0.09	pg/(ml day)	(38), fit	Falpha production by MI
alpha31	0.15	0.78	pg/(ml day)	(38), fit	Falpha production by MA
beta2	12000	12000	1/pg	(38), fit	Scaling factor of Mtb for Falpha production by MA
s10	100	300	pg/ml	(38), fit	Half saturation of IFNg on Falpha production by MA
alpha32	0.2	0.3	pg/(ml day)	fit	Falpha production by Th1
alpha33	0.2	0.3	pg/(ml day)	Fit	Falpha production by T8
nuTNF	1.1	1.1	1/day	(60)	Falpha decay rate
alpha19	0.87	1.27	1/day	(37), fit	BI replication rate
alpha20	0.3	0.4	1/day	(37), fit	BE replication rate
Nfracc	0.06	0.06	--	(37)	Fraction BI released by T cell apoptosis of MI
Nfraca	0.06	0.06	--	(37)	Fraction BI released by TNF apoptosis of MI
k15	0.0002	0.001	1/day	(37), fit	BE killing by MA
k18	0.0001	0.0007	1/day	(37), fit	BE killing by MR
nI	6.3E-05	8.3E-05	1/day	(38), fit	BI death rate
nE	4.4E-09	6.65E-09	1/day	(38), fit	BE death rate
Nfracd	0.001	0.001	--	fit	Fraction of BI released by natural death of MI

Table A1: ODE model parameters that govern individual granuloma formation and growth across time.

*For each disseminating granuloma, we allow for the option to sample each parameter from a subrange smaller than its parent's ranges. We do this by using a fraction between 0 and 1 (inclusive) to determine the limits of the range. The fraction represents the percent of values between the parent's value and either extrema (minimum and maximum) to include in the range. 0 means the range includes only the parent's value; 1 means that the original range is used.

Parameter name	Value	Units	Ref	Description
diamMacs	20	microns	(40)	Diameter of Macrophage
diamTCells	5	microns	(40)	Diameter of T cell
dt	1	day	~	Agent time step

Table A2: Other parameters for size of granulomas and runtime execution.

Parameter name	Min	Max	Units	Reference	Description
DissemDistMean	10^0	10^1	um	Fit, Based on data (25)	Mean distance of local dissemination
Lambda_Local	10^{-3}	10^{-1}	CFU/sec	Fit, Based on data (25)	Max probability of local dissemination
CFU_Half_Local	10^3	10^4	CFU	Fit, Based on data (25)	Value for half of max rate of local dissemination

Lambda_NonLocal	$10^{-3.5}$	$10^{-1.5}$	CFU/sec	Fit, Based on data (25)	Max probability of non-local dissemination
CFU_Half_NonLocal	$10^{3.5}$	$10^{4.5}$	CFU	Fit, Based on data (25)	Value for half of max rate of non-local dissemination
TcellFracDonateMu	1/100	1/10	--	estimated	Mean fraction of all of the parent granuloma's T cells that move to the daughter granuloma during a local dissemination event
TcellFracDonateSig	10^{-3}	10^{-2}	--	estimated	Standard deviation from the mean fraction of all of the parent granuloma's Tcells that move to the daughter granuloma during a local dissemination event

964 **Table A3: Dissemination Parameters.** These seven parameters dictate dissemination dynamics
965 in *MultiGran*. Parameters were fit to barcode data or varied using Uncertainty Analysis to find an
966 estimation.

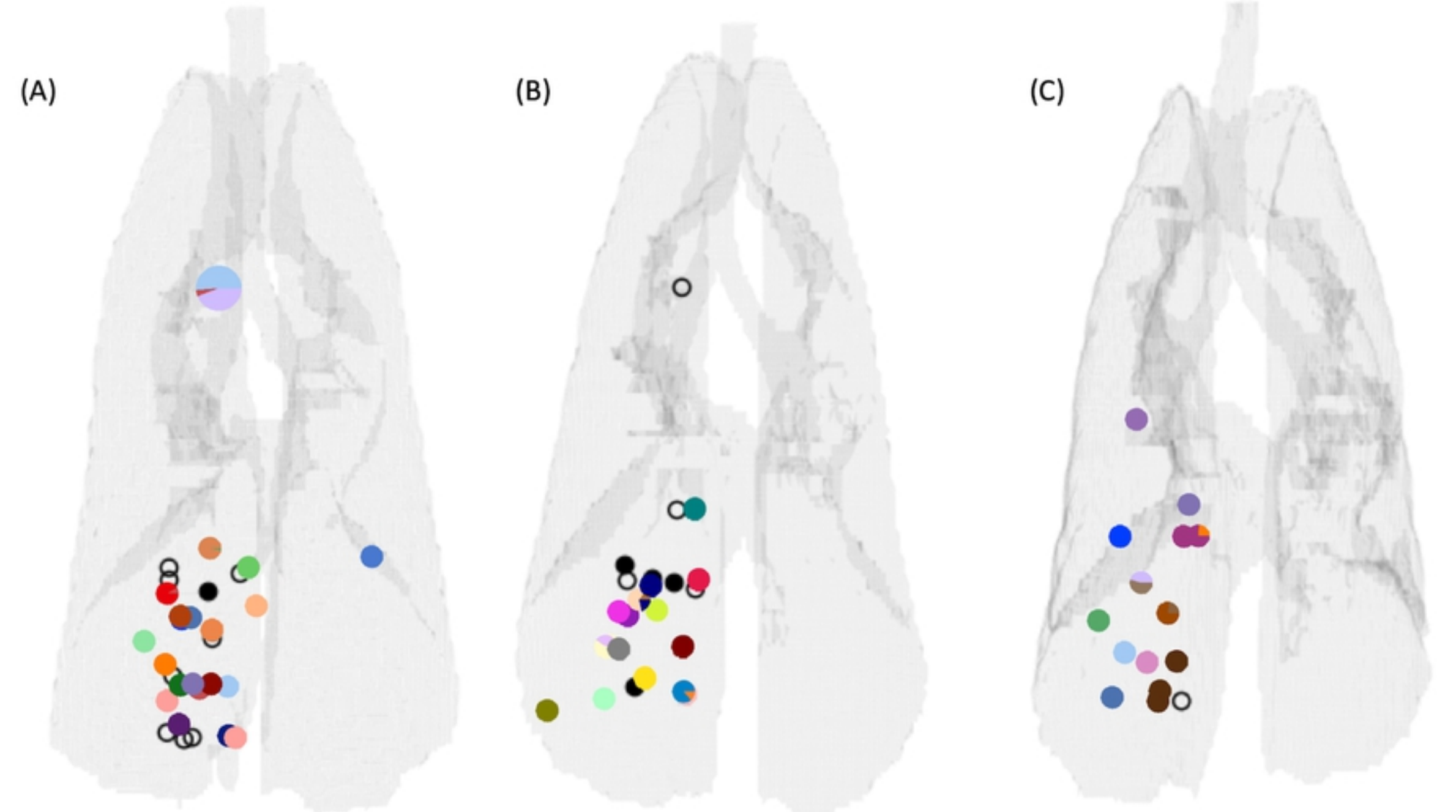

Figure 1

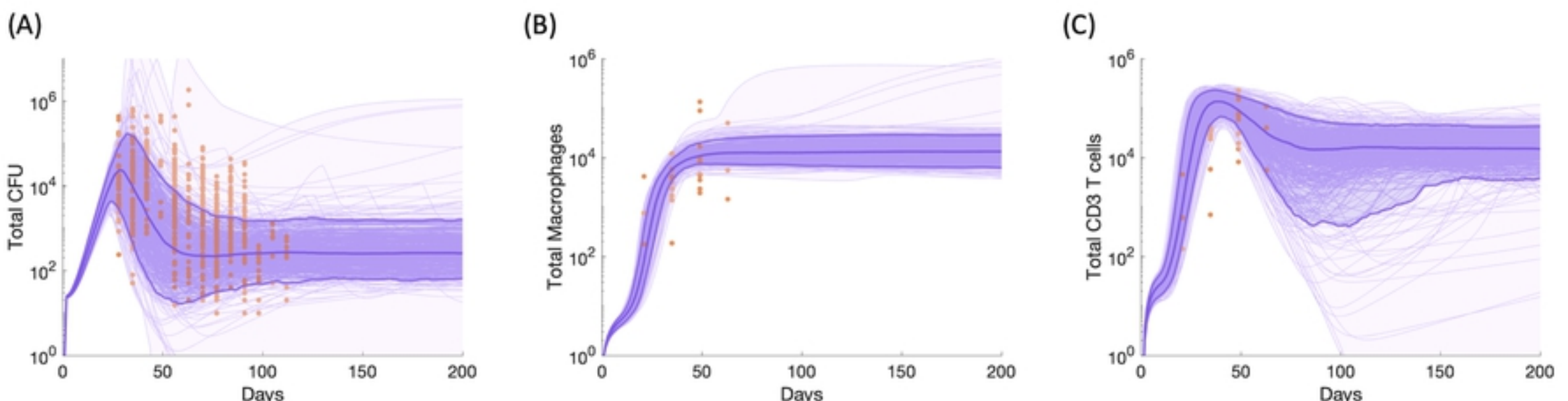
(A)
Total CFU
10^6
10^4
10^2
10^0
0
50
100
150
200
Days
(B)
Total Macrophages
10^6
10^4
10^2
10^0
0
50
100
150
200
Days
(C)
Total CD3 T cells
10^6
10^4
10^2
10^0
0
50
100
150
200
Days

Figure 2

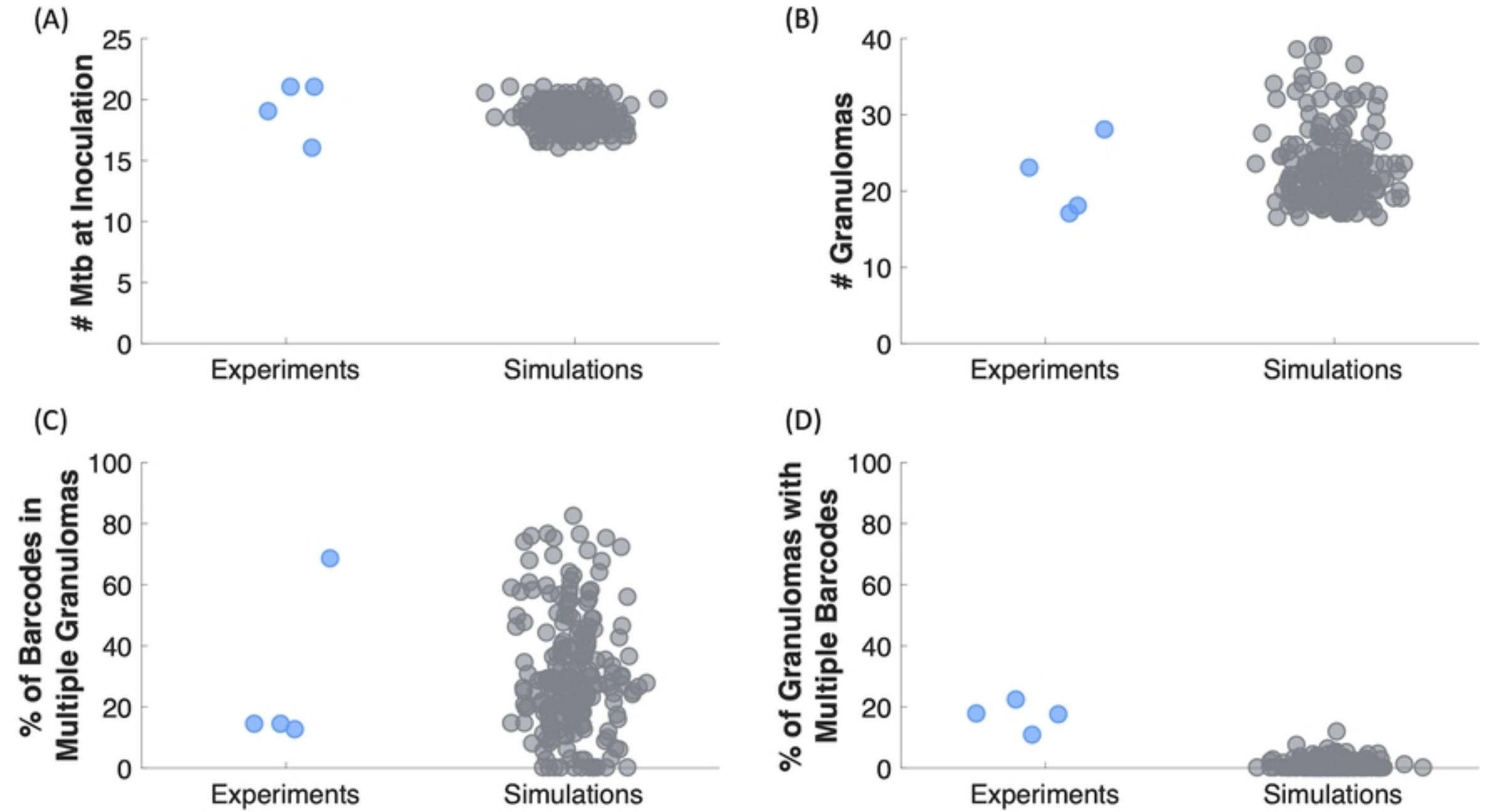
(A)
Mtb at Inoculation
25
20
15
10
5
0
Experiments
Simulations
(B)
Granulomas
40
30
20
10
0
Experiments
Simulations
(C)
% of Barcodes in Multiple Granulomas
100
80
60
40
20
0
Experiments
Simulations
(D)
% of Granulomas with Multiple Barcodes
100
80
60
40
20
0
Experiments
Simulations

Figure 5

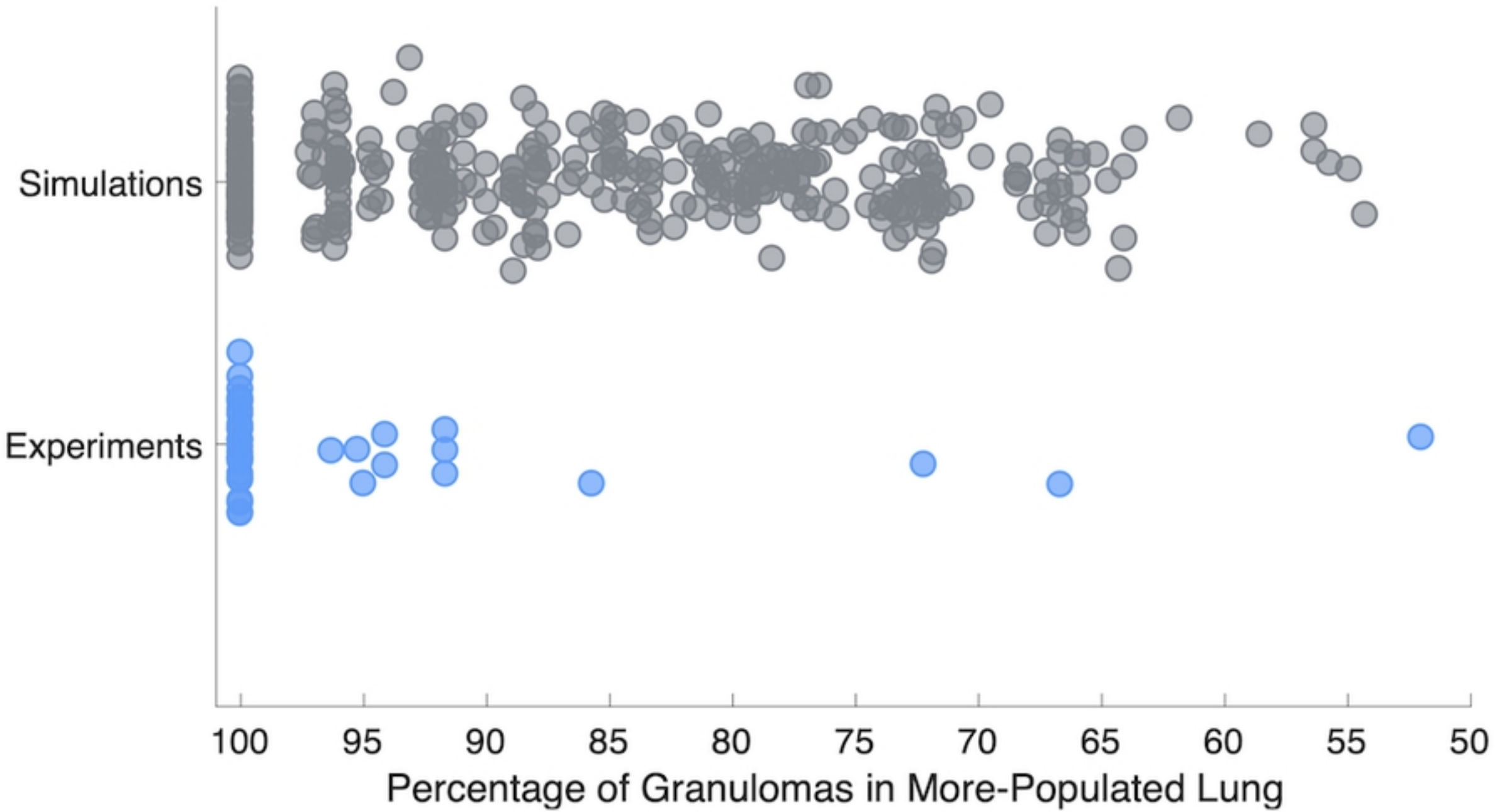
Simulations
Experiments
100
95
90
85
80
75
70
65
60
55
50
Percentage of Granulomas in More-Populated Lung

Figure 6

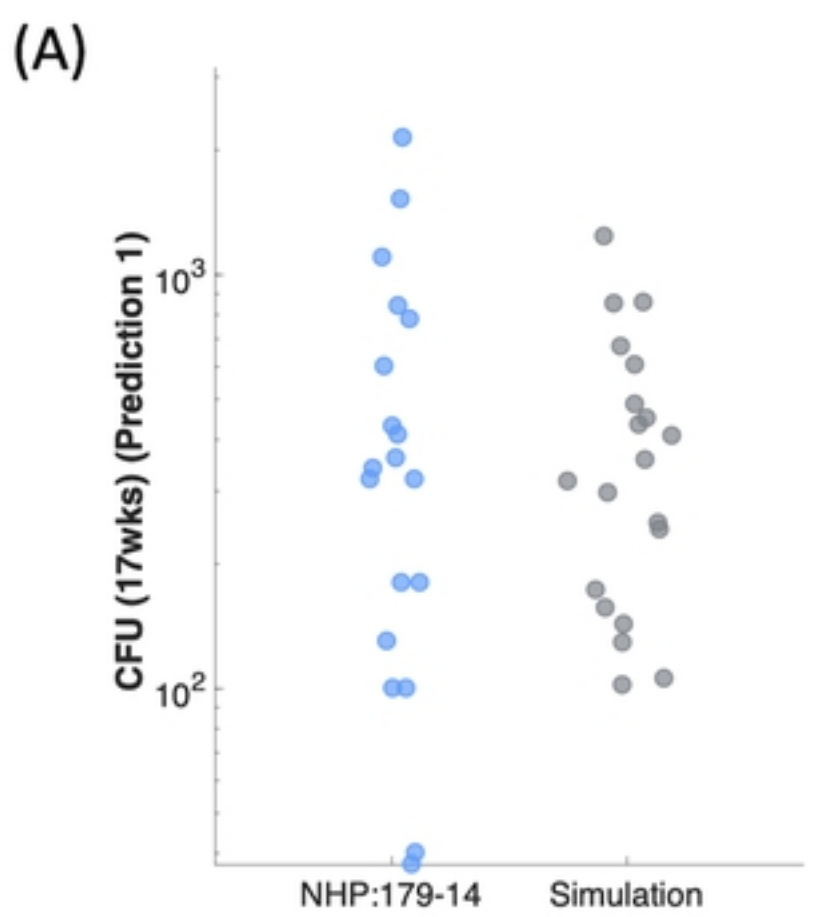
(A)
CFU (17wks) (Prediction 1)
10^3
10^2
NHP:179-14
Simulation

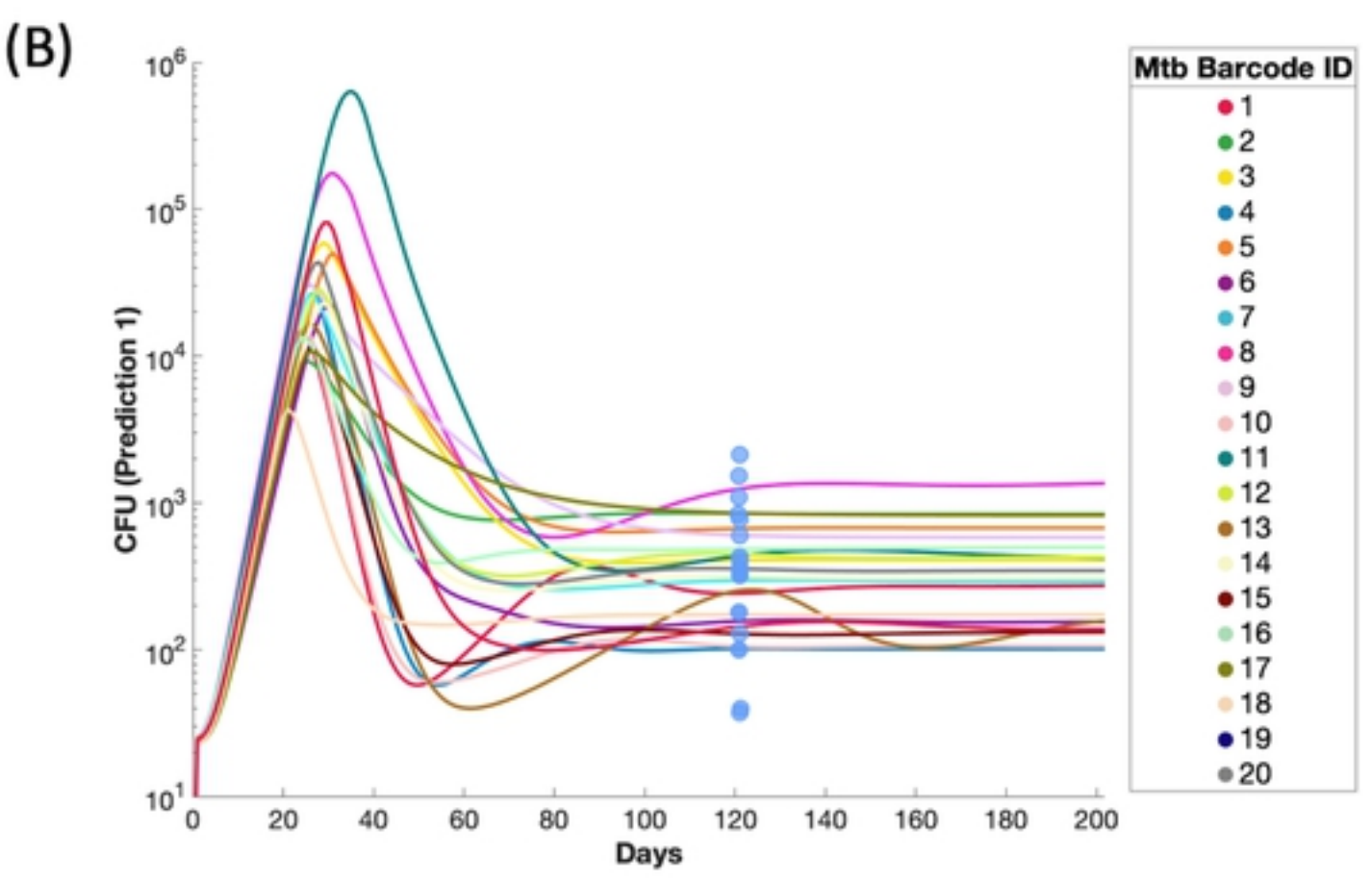
(B)
CFU (Prediction 1)
10^6
10^5
10^4
10^3
10^2
10^1
0 20 40 60 80 100 120 140 160 180 200
Days
Mtb Barcode ID
1 2 3 4 5 6 7 8 9 10 11 12 13 14 15 16 17 18 19 20

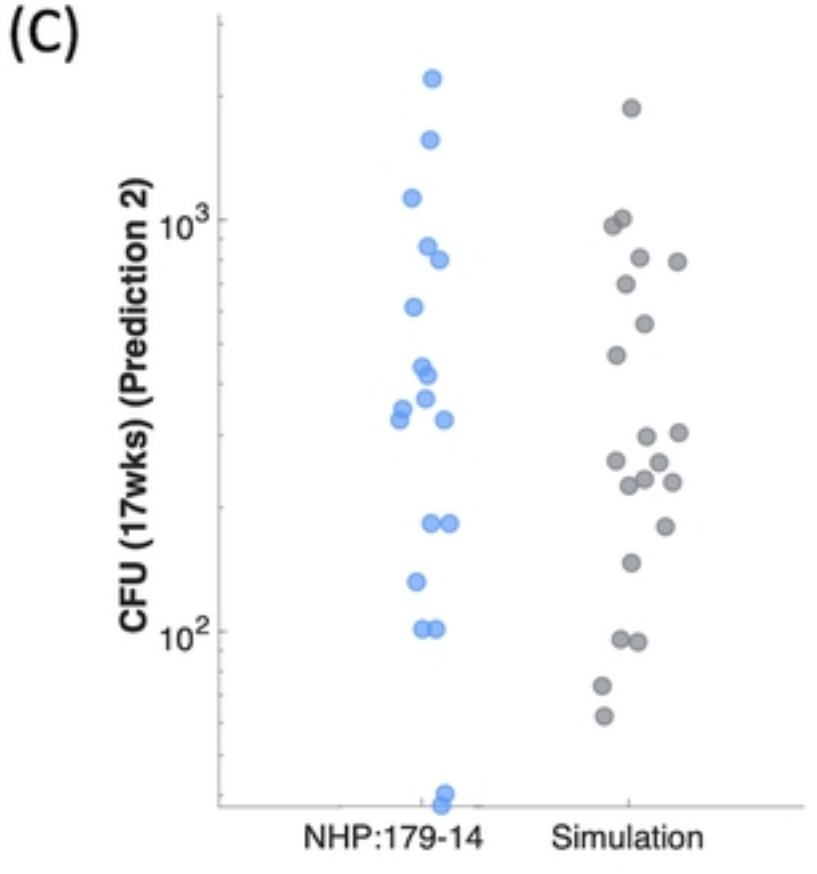
(C)
CFU (17wks) (Prediction 2)
10^3
10^2
NHP:179-14
Simulation

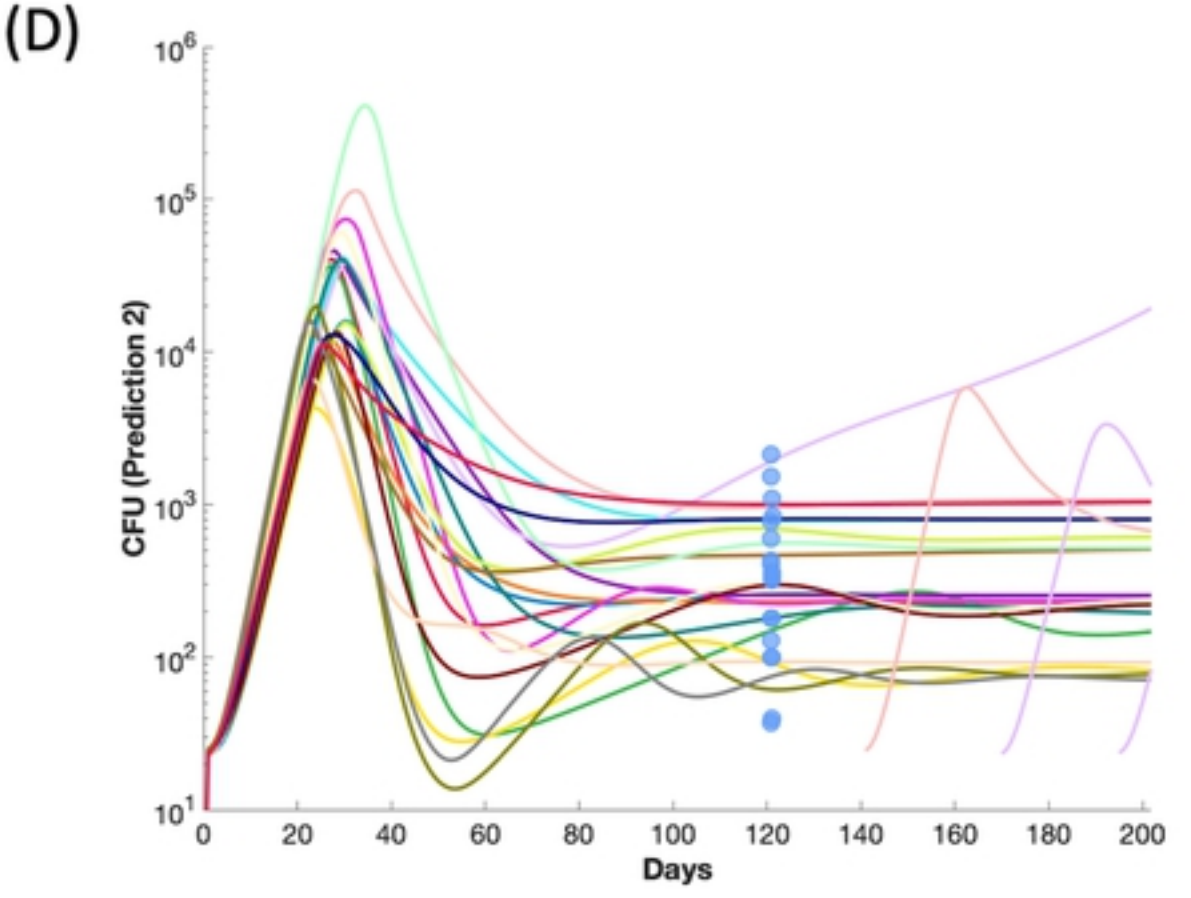
(D)
CFU (Prediction 2)
10^6
10^5
10^4
10^3
10^2
10^1
0 20 40 60 80 100 120 140 160 180 200
Days

Figure 7

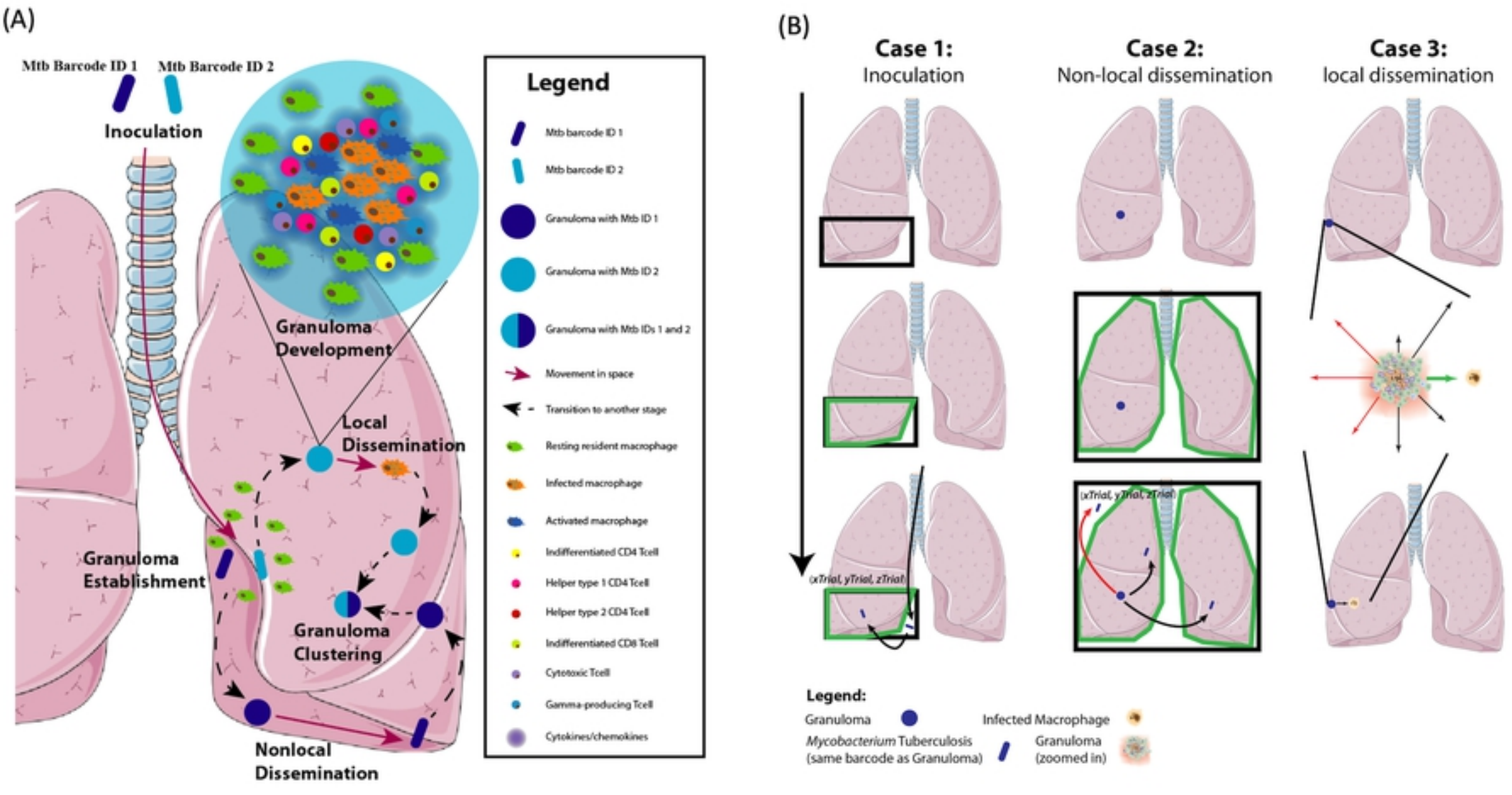
(A)
Mtb Barcode ID 1
Mtb Barcode ID 2
Inoculation
Granuloma Development
Local Dissemination
Granuloma Establishment
Granuloma Clustering
Nonlocal Dissemination
Legend
Mtb barcode ID 1
Mtb barcode ID 2
Granuloma with Mtb ID 1
Granuloma with Mtb ID 2
Granuloma with Mtb IDs 1 and 2
Movement in space
Transition to another stage
Resting resident macrophage
Infected macrophage
Activated macrophage
Indifferentiated CD4 Tcell
Helper type 1 CD4 Tcell
Helper type 2 CD4 Tcell
Indifferentiated CD8 Tcell
Cytotoxic Tcell
Gamma-producing Tcell
Cytokines/chemokines
(B)
Case 1:
Inoculation
Case 2:
Non-local dissemination
Case 3:
local dissemination
(xTrial, yTrial, zTrial)
(xTrial, yTrial, zTrial)
Legend:
Granuloma
Infected Macrophage
Mycobacterium Tuberculosis
(same barcode as Granuloma)
Granuloma
(zoomed in)

Figure 2

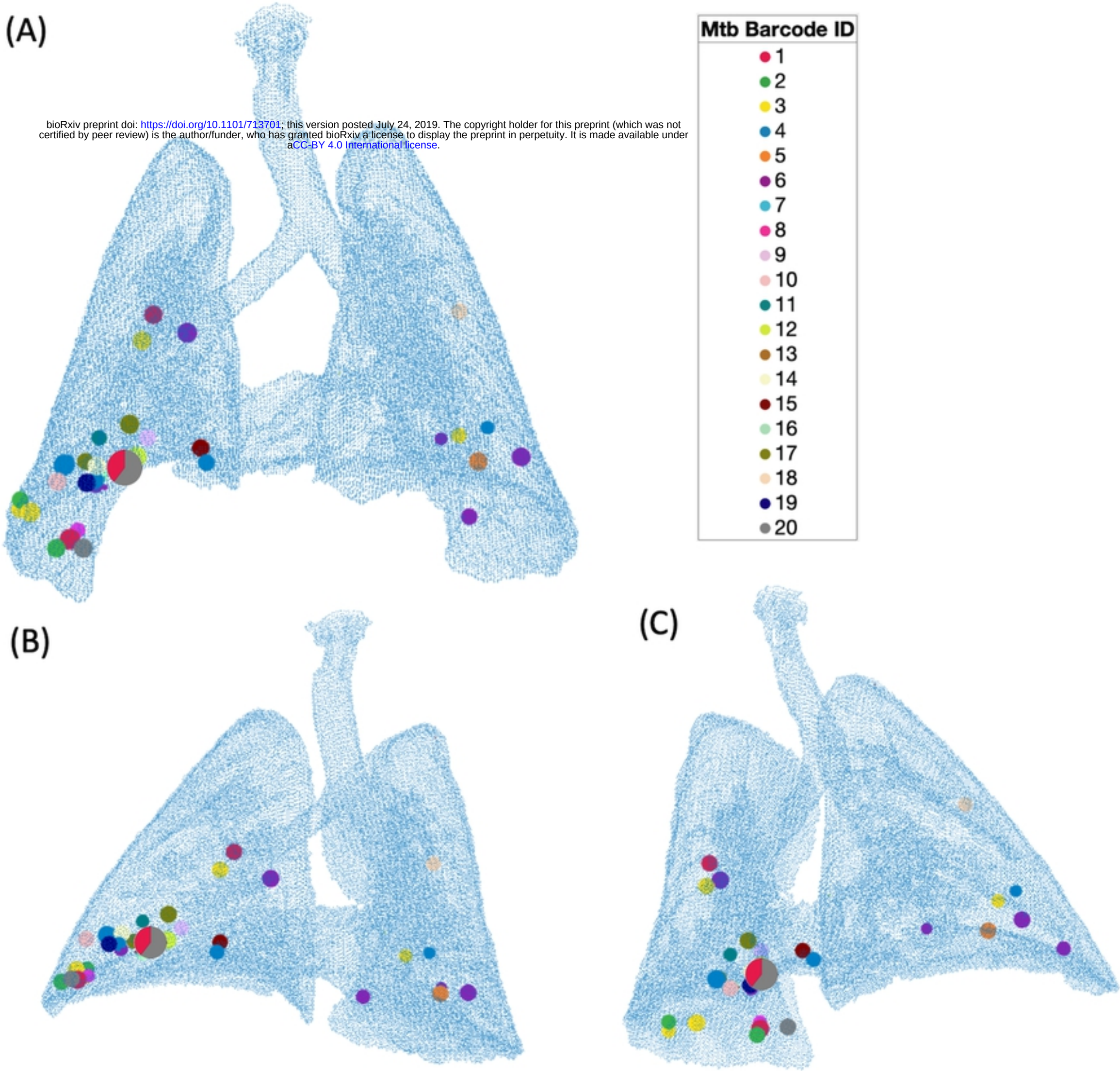

Figure 4